We warmly thank the three reviewers for their constructive comments which help to considerably improve the manuscript. This document is a point by point answer to each individual comment (referee comments italicised in orange), followed by the manuscript in which modifications from the original version are highlighted.

Anonymous Referee #1

Overall: This paper provides a description of the current GRISL1 ice sheet model, focusing on modifications and extensions from the previously described version in 2001. The model is designed for relatively coarse-resolution long-term paleo applications. Main change from 2001 include the specification of grounding-line fluxes (Schoof, 2007), and a basal hydrology model. A large ensemble with Latin Hypercube sampling is used to constrain and calibrate four uncertain model parameters. The paper is clear and provides useful supporting documentation for GRISL1 users and background for other papers on GRISL1 applications.

Specific comments:

1. There is considerable scatter in Fig. 7, showing pair-wise parameter correlations with the results (here, rms error in modern ice thickness). This may be because the Latin Hypercube (LHC) sampling of the large ensemble (LE) may be too coarse to meaningfully detect pair-wise dependencies. The quasi-random distribution of red, blue and green stars in these panels is reminiscent of corresponding figures in Applegate et al. (2012, The Cryo., their Fig. 1). Chang et al. (GMD, 2014) subsequently found that the scatter in the Applegate study is due to inadequate sampling in the high-dimensional parameter space, and they used additional statistical analysis with Gaussian emulation to extract meaningful dependencies (their Fig. 4a vs. 4b). That study had a similar number of parameters (5) and ensemble members (100) as here (4 and 150). In a similarly sized Antarctic LE, Pollard et al. (GMDD, 2016) found that meaningful dependencies could only be found with "full-factorial" sampling, i.e., a run for every possible combination of parameter values, requiring 5^4 = 625 runs for 4 parameters and 5 values each. If that many runs could be performed here, it might yield much more meaningful pair-wise results than in Fig. 7. However, if that would be too computationally expensive, it could be left to future work, and the above caveats could just be noted.

Encouraged by your concern we doubled the size of the ensemble. We now have 300 members for each formulation of the flux at the grounding line (600 members in total). Our ensemble is now considerably larger than the one of Applegate et al. (2012) considering that we have 4 parameters instead of 5. In addition, we have added the RMSE information in some figures (former Fig. 4 and Fig. 7) in order to facilitate the emergence of relationships. With this larger ensemble, the RMSE in the parametric space (new Fig. 7 and Fig. 8) mostly confirms what was suggested in the first version of the manuscript: there is generally no clear relationship between our parameters that can explain the RMSE with the major exception of the variable E_SIA versus C_f for simulations using Schoof et al. (2007) and E_SIA only for simulations using Tsai et al. (2015). From this, we suspect that to obtain meaningful dependencies we should in fact probably expand drastically the ensemble, probably by doubling again its size (order of magnitude from 10^2 to 10^3). This is beyond the scope of the manuscript but we acknowledge the fact that emulators trained with very large ensemble are a very promising field of applications for large scale ice sheet model.

2. The simulations here use uniformly prescribed basal drag coefficients, and do not use an inversion method to deduce a spatial map. There is discussion on the pros and cons (pg. 6, 15, 17),

which makes good points for not using inverse methods. But it does not mention the primary motivation (I think) for using them: that without them, modern errors in ice thickness are much larger (as in Figs. 5,6), and can be made much smaller using an inverse procedure. Since these errors are the primary metric here for evaluating the model, this could help to make the calibration of model parameters more meaningful. I think the whole issue depends on whether the inverse-produced map captures real bed variations at all, or if it just cancels with and obscures other physical errors in the model. I suggest mentioning this within the existing discussion. Also, the point made on pg. 17, line 16, on the desirability of making basal coefficients a property solely of internal model parameters (such as N here, in Eq. 14), is debatable: apart from basal temperatures and water amount of course, spatial variations in basal sliding can also depend importantly on geologic bed type, roughness, and the distribution of deformable till, which are outside the scope of the model.

The simulations in this paper do not use uniformly prescribed basal drag coefficients as they are computed from the effective water pressure that varies both in space and time (Eq. 16). This is precisely the capability of this formulation to respond interactively to changes in geometry that motivated our choice over an inverse method.

Using an inverse method to infer the basal drag coefficients would not help in calibrating the model parameters because, by construction, the inverse method will correct any bias in both the forcings (climate/bedrock) and the model physics. For example, for different enhancement factor values we can, in principle, infer different basal drag coefficients maps that will result in close-to-observation geometry.

We have nonetheless added a sentence on the pros of inverse methods (Sec. 2.1.3):
“Inverse methods are particularly adapted to produce an ice sheet state (e.g. geometry and/or velocity) close to observations. However, such methods do not provide [...]”

About a basal drag computed from internal variables only, you are right mentioning the importance of bed properties such as geologic bed type and roughness. These are largely uncertain both in term of their values and in term of their impact on ice dynamics. We have slightly modified these lines:

“A step forward would be to use the basal drag computed from inversion in order to deduce a formulation based solely on internal parameters. Amongst these parameters, along with the basal effective pressure, the large scale bedrock curvature and/or sub-grid roughness could be used, similarly to Briggs et al. (2013). However, some key basal features, such as the geologic bed type and the deformable till distribution, remain today largely unknown below present-day ice sheets and will contribute to large uncertainties in the basal drag formulation.”

3. In Eq. 14 on pg. 6, and section 2.2.1 (Eqs. 24-26, pg. 9), it is not clear how some variables for basal hydrology are determined: h_w or p_w (which are related, line 24), and effective pressure N needed for Eq. 14. Presumably there is a prognostic equation in the hydrology model for h_w, i.e., d(h_w)/dt = ..., that is not shown here. Perhaps it is the equation mentioned on pg. 9, line 23. Also N possibly depends on p_w. This information, and the equation for h_w, should be included. (Incidentally, if N depends on depth below sea level as in several other models, I would question how can it reasonably depend on that, at distances 10’s or 100’s km inland from the grounding line).

We acknowledge that the original description of the hydrology was somehow incomplete and we have considerably rewritten this section with clarity in mind. The prognostic equation for the

hydraulic head h_w is now presented. We also explicitly mention how we compute p_w and N from h_w. N does not depend explicitly on the depth below sea level as it is computed as the difference from the ice load pressure (rho_i g H) and the basal water pressure (rho_w g h_w). However, the depth below sea level is a necessary boundary condition for the hydraulic head at the marine ice sheet margin (h_w=sealevel-Bbed).

4. The determination of buttressing factor phi_bf in Eq. 15 (pg. 7) is an important part of the use of the Schoof flux equation, but the procedure is unclear to me from lines 21- 25 on that page. Perhaps the first solution provides the back-stress-free solution...does that solution use Eq. 15 with phi_bf = 1? Then what is the second solution, and where does its value of phi_bf come from? These questions may not make sense, and just show my confusion. Hopefully this paragraph can be clarified, and perhaps expanded if that would help.

We acknowledge that it was not clear in the first version of the manuscript. In fact, in our framework we compute the velocity equation three times with the two first iterations being used to compute phi_bf. The first iteration is computed on the simulated geometry with no flux adjustment at the grounding line. The second iteration is computed the same way, except for the fact that the ice shelves are assigned to a very low viscosity so that they cannot exert any back force. The buttressing ratio phi_bf is then computed as the velocity ratio between these two computed velocities. The flux adjustment at the grounding line is only applied for a third iteration which gives us the actual velocity field. We have made this clearer in the manuscript:

“To evaluate the back force coefficient phi_bf, we solve the velocity equation twice. The first iteration is computed on the simulated geometry with no flux adjustment at the grounding line (i.e. not using Eq. 17 nor Eq. 18). The second iteration is computed the same way, except for the fact that the ice shelves are assigned to a very low viscosity so that they cannot exert any back force. The buttressing ratio phi_bf is then computed as the velocity ratio between these two computed velocities. Once phi_bf is estimated, we solve the velocity equation again, this time accounting for the flux ajustment at the grounding line using Eq. 17 or Eq. 18, in order to estimate the velocity used in the mass conservation for this time step.”

We acknowledge for the fact that the two first iterations produce unrealistic simulated velocities as they do not account for any specific treatment at the grounding line. However, we assume that the ratio in velocities is representative for the buttressing effect of ice shelves.

5. pg. 16, lines 5 to 7: Perhaps, the timings of the deglacial retreat in AN40T vs. AN40S can be assessed vs. papers in the RAISED reconstruction volume (Bentley et al., 2014), or other data, in order to determine which one is more realistic. The paper seems to decide rather arbitrarily that the AN40T case is more realistic (pg. 18, line 25).

The fact that the model is still drifting at +10 kyr in the future with AN40S is a clear indication of a too slow retreat in this case. However, it is true that our climatic forcing is relatively simple and that with an alternative climate forcing we could maybe have a faster retreat with AN40S. Keeping that in mind, we have moderated this sentence:
“This suggests that, in our model and under the climate forcing scenario we use, the Tsai et al. (2015) formulation produces a more realistic grounding line retreat rate. ”

There is unfortunately no archive that allows for an ice volume change reconstruction of the Antarctic ice sheet during the last deglaciation. While, the RAISED reconstructions do not quantify

the change in ice volume, it is indeed nonetheless, at present, the most complete data compilation on the extent of the grounding line during the last deglaciation. However, the temporal resolution (5 kyr) together with the fact that the largest uncertainties remain in the Weddell and Ross seas, make it difficult to compare with our model results. This is why although we discuss the RAISED reconstructions in the original version of the manuscript for the ice extent at the last glacial maximum, we did not use this as a constraint for the timing of the deglaciation.

6. pg. 13, lines 9-10: The pairs of values "1.5 to 3" and "1.5 to 5" do not seem to relate to the bottom-right panels in Figs. 3 and 4, for basal-drag coefficients K0 (which are being discussed in that sentence). They seem to relate better (but still fuzzily) to the bottom-left panels for enhancement factors E_sia.

The initial formulation was misleading as we were indeed referring to the enhancement factors. We reformulated as:
"As a consequence, for the AN40T ensemble, the enhancement factor requires values between 1.5 and 3 in order to reach a good agreement with observed ice thickness, whilst values within 1.5 to 4 are acceptable for AN40S."

Technical comments:

The English usage is generally good, but isolated words or phrases could be improved/corrected, some of which are noted below.

pg. 1, line 19: Change "are evidences" to "is evidence".

Done.

pg. 1, line 23: Change "An other" to "Another".

Done.

pg. 2, line 7: I think "prograde" should still be "retrograde", for MICI as well as for MISI.

We acknowledge the fact that a retrograde slope will inevitably amplify both the MISI and MICI. However, as postulated by Pollard et al. (2015) and contrary to the MISI, the MICI can also occur on neutral and prograde slopes. We clarified this sentence:
"Additional instabilities may also occur on neutral/prograde bed slopes in relation with the structural instabilities of tall ice cliffs (marine ice cliff instability, MICI, Pollard et al., 2015)."

pg. 2, line 23: The word "diffusion" should probably be removed (?).

Removed.

pg. 3, line 14, and several later places: "Tab. 1" should perhaps be "Table 1".

The GMD manuscript preparation guidelines for authors suggest to use abbreviations (Sec., Fig., Eq., Tab.) when used in running text unless it comes at the beginning of a sentence. We have followed these guidelines consistently.

pg. 4, line 1: The use of two "respectively"'s in the same sentence is confusing - perhaps divide into 2 separate statements for sigma_i and tau_ij.

It has been changed to:
"[…] where tau_ij=x,y,z are the shearing stress tensor terms and sigma_i=x,y,z the longitudinal stress tensor terms, defined as (i=x,y,z):
sigma_i = tau_ii"

pg. 4, line 26: Change "Alike" to "Like".

Done.

pg. 4, lines 27-29: The word "reduces" in line 27 seems to contradict the word "favour" in line 29. Or perhaps "longitudinal" should be "shearing" in line 29 (?).

Thanks for noticing, it was effectively a mistake. This part has been expanded and reformulated.

pg. 5, line 24: What does "see also numerical feature" mean?

Changed in the text to:
"[…] see also Sec. 2.3 on the numerical features"

pg. 16: I would suggest emphasizing, as a positive note, that if the (interpolated) grounding line position is known, then all that is required to obtain ice thickness H_gl at the grounding line for Eq. 15 is (1) bedrock bathymetry interpolated to the grounding line position, and (2) sea level. (This is because of the floatation criterion at the grounding line of course).

The sub-grid position of the grounding is known because we linearly interpolate the floatation criteria based on the knowledge of thickness, bathymetry and sea level on the centred GRISLI grid. For more clarity for the reader, we have added a schematic representation of the staggered grids (Fig. 2) and expanded the description of how we apply the grounding line flux on the velocity nodes.

pg. 10, line 23-24: Explain the need for the artificial extension (to get an ice front parallel to x or y).

With this extension, the front of the ice shelf is always parallel to either x or y which facilitates the application of boundary conditions. This is now explicitly stated in the manuscript. A schematic representation of the different cases for the elliptic equation is now shown in Fig. S1 of the supplementary material.

pg. 11, line 20: Misspelled "projet".

Corrected.

pg. 12, line 15: "in 150" should be "of 150".

Changed.

pg. 12, line 20: Perhaps change "are discarded from" to "are not included in" ?

It has been changed to “are not explored in”.

pg. 14, line 6: Change "somehow" to "somewhat".

Done.

pg. 15, line 16: Does this mean that a 100-kyr long spinup is performed with perpetual modern climate for every ensemble member? If so, say that more clearly.

All the ensemble members (300x2) in Sec. 3 are 100-kyr integrations of the model using perpetual modern climate (p.11 l.16-17 in the initial manuscript). The spun-up ice sheet used for the transient simulations is the final state obtained at the end of the 100-kyr integration in Sec. 3. For sake of clarity, we reformulate as:
“We used the 100-kyr integration under perpetual modern climate in Sec. 3 as a spin-up for the transient simulations.”

pg. 15, line 24: The range of 10 to 20 m eustatic sea level drop here is actually a bit larger than several recent model studies. This might be due to larger basal drag coefficients used here on modern continental shelves, so when grounded ice expands onto them at LGM, the expanded ice is thicker there.

The reviewer is perfectly right here. During glacial periods, the ice sheet expands onto part of the continental shelf that presents presumably different bedrock conditions. In particular, we can expect to find more deformable till relative to hard bed in these areas, facilitating the ice flow for large part of today ice-free regions. For these reasons, some authors choose to use a two-value basal sliding coefficient for hard bedrock (bedrock above sea level) and deformable sediments (bedrock below sea level) (e.g. Pollard and Deconto, 2012). Because geologic information below present-day Antarctica is poor, we have preferred to keep our approach as simple as possible with no additional tuning. However, for future work it is clear that sensitivity studies on the role of bedrock characteristics will have to be performed.

Following your comment, we have added the following in the manuscript:
“Our reconstructions are nonetheless at the higher hand of recent studies. This could be related to the fact that we do not account for different geologic bed types between today ice-free (with extensive amount of deformable till) and glaciated (mostly hard bed) continental shelf. To account for this, some authors have chosen a two-value basal drag for these different regions (e.g. Pollard and Deconto, 2012). Because of the large uncertainties related to the bed properties we have decided to ignore these differences, keeping in mind that this can bias our results towards thicker ice sheet when the ice expands over the continental shelf.”

pg. 16, line 4: Change "In turns" to "In turn".

Done.

pg. 17, line 2: "using an inverse method" sounds like one is used here. Make it clear that one is not, and that phrase refers just to the references earlier in the sentence.

This now reads:

“We have presented results from the updated version of the GRISLI model. Whilst the model is able to reproduce present-day Greenland (Le clec’h et al., 2017) and Antarctic (Ritz et al., 2015) ice sheets when using an inverse method to estimate the basal drag, our simulations with an interactive basal drag computed from the effective pressure show some important disagreements relative to observations.”

Table 1: Some of these variables do not seem to be used in the text, e.g., those under "Deformation". Others may have a different name, e.g., h_till.

We have now given more information on the computation of the viscosity in the model and we refer explicitly to the variables listed below “deformation”. We have checked the table carefully and corrected a few mistakes. If some of the variables here are effectively not used in the text, in particular the ones for the isostatic rebound model, we have nonetheless preferred to keep them here for documentation of this particular version of the model.

Fig. 2: The relationship between the sector boundaries (left-hand panel) and the contour divisions for basal melt rates (right-hand panel) is confusing, not as one might expect. That is, there seems to be some divisions between the colors in the right-hand panel that are not present in the left-hand panel, and vice-versa.

We imposed a specific (high) sub-shelf melting rate for the deep ocean (depth greater than 2500 m). This is why one region (deep ocean) of the right-hand panel does not appear on the left-hand panel. We now explain this in the text:
“Sub-shelf melting rate for the deep ocean (depth greater than 2500 m) are assigned a value of 5 m/yr.”
Also, if some sectors that appear on the left-hand panel do not appear on the right-hand panel this is because they have the same or similar sub-shelf melting rates and cannot be distinguished.

References

Pollard, D. and DeConto, R. M.: Description of a hybrid ice sheet-shelf model, and application to Antarctica, Geosci. Model Dev., 5, 1273-1295, https://doi.org/10.5194/gmd-5-1273-2012, 2012.

Pollard, D. and DeConto, R. M. and Alley, R. B.: Potential Antarctic Ice Sheet retreat driven by hydrofracturing and ice cliff failure, Earth and Planetary Science Letters, 412, 112-121, https://doi.org/10.1016/j.epsl.2014.12.035, 2015.

Bentley, M. J., Ó Cofaigh, C., Anderson, J. B., Conway, H., Davies, B., Graham, A. G. C., Hillenbrand, C.-D., Hodgson, D. A., Jamieson, S. S. R., Larter, R. D., Mackintosh, A., Smith, J. A., Verleyen, E., Ackert, R. P., Bart, P. J., Berg, S., Brunstein, D., Canals, M., Colhoun, E. A., Crosta, X., Dickens, W. A., Domack, E., Dowdeswell, J. A., Dunbar, R., Ehrmann, W., Evans, J., Favier, V., Fink, D., Fogwill, C. J., Glasser, N. F., Gohl, K., Golledge, N. R., Goodwin, I., Gore, D. B., Greenwood, S. L., Hall, B. L., Hall, K., Hedding, D. W., Hein, A. S., Hocking, E. P., Jakobsson, M., Johnson, J. S., Jomelli, V., Jones, R. S., Klages, J. P., Kristoffersen, Y., Kuhn, G., Leventer, A., Licht, K., Lilly, K., Lindow, J., Livingstone, S. J., Massé, G., McGlone, M. S., McKay, R. M., Melles, M., Miura, H., Mulvaney, R., Nel, W., Nitsche, F. O., O’Brien, P. E., Post, A. L., Roberts, S. J., Saunders, K. M., Selkirk, P. M., Simms, A. R., Spiegel, C., Stolldorf, T. D., Sugden, D. E., van der Putten, N., van Ommen, T., Verfaillie, D., Vyverman, W., Wagner, B., White, D. A., Witus, A. E., and Zwartz, D.: A community-based geological reconstruction of Antarctic Ice Sheet

deglaciation since the Last Glacial Maximum, Quaternary Science Reviews, 100, 1-9, https://doi:10.1016/j.quascirev.2014.06.025, 2014.

F. SAITO (Referee #2)

This paper describes the numerical ice-sheet model GRISLI ver 2.0, in particular, with the application for the Antarctic ice sheet simulation. I think this paper is fairly well written with some exception below, and can be accepted with minor revision.

One thing better to include is technical (numerical) procedures and properties adopted in the model. Since the source code is not opened to public, information how to solve the model equation is useful for those who has not contact with the model. For example, how to solve the Eq.(2), (thickness evolution)? Explicit, implicit or others? How to solve the linear equations, direct, alternate-direction, conjugate gradient, or other method? How to solve the non-linear ice-shelf equation (Eq.12)? Linearize them? Or the velocity-dependent viscosity (\bar{eta}) at the previous time step is used? How to determine the convergence of the solutions where the iterative solver is involved? Such details are all necessary to evaluate the numerical accuracy of the model, if they want. I suppose they are more or less the same as the original version of the model (Ritz et al. 1997,2001), but repetition (or at least citation of the old papers) are needed for completeness of the model description.

This is perfectly in line with Referee #3 general comment and we acknowledge that the initial version of the paper provided only few technical information. In the revised version, we now explicitly show the staggered grid in Fig. 2. We have also added two additional figures in the supplementary material showing: i) the boundary conditions when extending the front to the edges of the geographical domain and ii) the matrix used to solve the elliptic equation. We have also considerably expanded Sec. 2.3, adding more information on the numerical resolution of the equations:

“The mass balance equation is solved as an advection-only equation with an upwind scheme in space and a semi-implicit scheme in time (velocities at the previous time step are used). The numerical resolution is performed with a point-relaxation method with a variable time step. The value of this time step is chosen to ensure that the matrix becomes strongly diagonal dominant to achieve convergence of the point-relaxation method. The criteria is thus a threshold that is inversely proportional to the fastest velocity on the whole grid. Note that this smaller time step is solely used for the mass conservation equation and subsequent variables (e.g. surface slopes, SIA velocity) while the rest of the model uses a main time step, typically ranging from 0.5 to 5 years depending on the horizontal resolution.

To solve it, the ice shelves/ice streams equation (Eq. 14) is linearised. The viscosity is computed using an iterative method starting from the viscosity calculated from strain rates from the previous time step. As this equation is the most expensive part of the model, the iteration mode is not always used depending on the type of experiment (for instance not crucial when the objective is to reach the steady state). In this case the viscosity of the previous time step is used. The linear system is solved with a direct method (Gaussian elimination, sgbsv in the Lapack library (www.netlib.org/lapack)).

For the temperature equation (Eq. 19), we solved a 1D advection-diffusion equation for each model grid point. The resolution is performed with an upwind semi-implicit scheme (vertical velocity and heat production at the previous time step is used). The ice thermal conductivity is computed as the geometric mean of the two neighbouring conductivities (Patankar, 1980). Because the horizontal diffusion is neglected, the only horizontal terms concern horizontal advection and are computed

with an upwind explicit scheme. The heat production is computed at the velocity (staggered) grid points and is then summed up to the temperature (centred) grid points."

Another thing better to rewrite is the lateral boundary condition of the ice shelf, which is still unclear to me. As described in Sec 2.3, the ice shelf is extended towards the edges of the model domain. As far as I understand, to remove row i from the matrix corresponds to set horizontal velocity as zero at the front.

No, it does not mean that horizontal velocity at the front is zero, it means that it has an undefined value.

I am not sure this is what the authors expect. I suggest to rewrite the second paragraph of the Sec.2.3 to clarify how to formulate the matrix in the model.

We now show the matrix in the supplementary material and we have been more specific in the revised version, which now reads:

"The resolution of the elliptic system (Eq. 14) is the most expensive part of the model. This is further amplified by the way we prescribe boundary conditions. As in Ritz et al. (2001), the ice shelf region is artificially extended towards the edges of the geographical domain. This artificial extension does not have any consequence on ice shelf velocity since added grid points (that we call "ghost" nodes) are prescribed with a negligible ice viscosity (1500 P a s). The front is then parallel to either x or y (Ritz et al. 2001) and thus the boundary condition there is easy to implement (see also Fig. S1 in the supplement). The boundary condition at the real ice shelf front is implicitly done by solving (Eq. 14). However this method increases substantially the size of the linear system solved in (Eq. 14). To go around, a simple reduction method is implemented. Eq. 14 can be written as $\tilde{A}\,\tilde{\mathbf{u}} = \tilde{B}$ where $\tilde{\mathbf{u}}$ is a vector alternating u_x and u_y components for all the velocity grid points, $\tilde{A}$ is a band matrix (very sparse) and $\tilde{B}$ is a vector corresponding to the right hand terms in Eq. 14. Every line of $\tilde{A}$ and $\tilde{B}$ are scaled so that the diagonal terms of $\tilde{A}$ are equal to 1. If, for a given velocity node, all the non diagonal terms of the column are very small compared to 1, this means that this node is actually not used by any other velocity node and this line of the matrix can be removed. The threshold to neglect nodes is related to the value of the integrated viscosity of "ghost" nodes . In practice, given its size, the matrix $\tilde{A}$ is not actually fully constructed, only the non zero sub/sur diagonals are. An illustration of the matrix is shown in Fig. S2 in the supplement. "

In addition, I definitely agree to the specific comments 3 and 4 by the referee #1. The authors should clarify the formulation and the procedures to compute basal hydrology and the back-force coefficient.

The basal hydrology is now presented in much more details, including the prognostic equation for the hydraulic head, h_w, from which the effective pressure is computed. We have also clarify in the revised version how the back-force is calculated (please see also our response to the 4th point of referee #1).

Some minor points (PmLn corresponds to the line number n in page m)

Units: use \unit{} macro.

Thanks for the suggestion, we have done so.

P1L6: 'or Tsai et al....' may be better?

Changed.

P2L16: 'right' might not be a right word for this context. How about 'practical tool for....'

This has been replaced by "the most suitable tool for".

P3L19 Eq(1): Divergence, not Gradient (need dot).

We have followed this convention consistently in the text.

P3L22 Eq(2) and after: \bar{u}_x is better than \bar{u_x}.

Changed.

P3L26 Eq(3) and similar array equations: Use \displaystyle.

We have followed your suggestion.

P4L1 or around: Need definition like \sigma_i = \tau_{ii}, otherwise the paper misses the equation for longitudinal stress components, since Eqs 5, 6, 8, 9 are described with \tau_{ij}.

We agree, this has been added.

P4L11 Eq(7) or (9): The enhancement factor should be inserted. Otherwise E_{SIA} in P12L1 is confusing.

We have now added the equation for B_{AT} in which the enhancement factor appears (renamed as Sf for consistency with Ritz et al., 1997 and to avoid confusion with the activation energy Ea).

P4L16 Eq(8): Need range of i,j.

Information added (i,j={x,y,z}).

P4L25 Eq(9): No explicit formulation of B_{AT1} and B_{AT3}. Are they documented in Dumas (2002)?

We have added the equation for B_{AT} and expanded the description of how they are calculated for the Glen viscosity and the linear viscosity. We hope that the new version of the manuscript contains all the necessary information.

P5L10 Eq(10): i in \rho_{i} conflicts with row i.

The density of ice is simply referred as rho consistently in the whole manuscript.

P5L9: (for i = x,y) not (for i=x,y,z). When i=z in Eq(11), the coefficient 2 must disappear.

Thanks for noticing, this has been corrected now. Vertical velocity is mentioned later in the manuscript.

P5L10 Eq(11): no definition of B. B may conflict with B_{AT}, which is better to avoid.

We have added the definition of B (bedrock elevation). We stick to B and B_{AT} for consistency with Ritz et al. (2001).

P5L21: S is already defined in L9.

Thanks for noticing, the definition here has been removed.

P5L23: (see also 2.3 numerical feature)

Changed in the text to:
"[…] see also Sec. 2.3 on the numerical features"

P5L26: The basal drag is very small but not necessarily zero. All we can do is to neglect it.

We agree, we now simply say that we neglect it.

P7L12 Eq(16): No definition of H_g. Typo of H_{gl}?

Thanks for noticing, we meant H_{gl}.

P8 Sec2.1.6. Need to mention how to compute the vertical velocity. I suppose vertical velocity is not directly computed as Ritz et al. (1997).

Vertical velocity is indeed computed as in Ritz et al. (1997). We added this information in the text :
"u_z is the vertical velocity, computed as in Ritz et al. (1997) (wt in Eq. 14)."
This velocity is used for 3D advection (temperature and tracers).

We have also added more information on the link between temperature and viscosity:
"The viscosity for the velocity grid points is the horizontal average of the viscosity on the centred grid and not the viscosity computed from the horizontal average of the temperature. This is preferable for regions with mixed frozen and temperate basal conditions."

P8L10: 'zero' requires the unit. I prefer to write as 'the melting point'.

True, it has been changed.

P8L25 Eq(22) Write \exp (backslash before exp) following LaTeX convention.

Done.

P9L27, Better to cite Le Meur and Huybrechts after ELRA sentence also.

Done.

P10L26: Better to avoid to use A and B for matrix and vector, which conflict with the rate factor or bedrock elevation.

Most of the letters in the alphabet relate to a variable used at some point in the model. We think that A and B, being the first letters, are more generic. We have nonetheless added a tilde (~) on top of them for a better distinction with respect to the rate factor and the bedrock elevation.

Table 1: Unit of the acceleration should be m/s. Really same values for ice and mantle thermal conductivity?

Thanks for noticing this. We changed the unit of the acceleration and we corrected the ice thermal conductivity.

Figure 1: If z at the ice bottom is always zero as the figure, you need to reformulate all the governing equations using z.

Sorry for this, z should have been B at the ice bottom and S=B+H at the top. The figure has been updated.

Anonymous Referee #3

Summary: This paper describes a new version of the GRISLI ice sheet model, including new model development since an earlier version many years ago (Ritz et al., 2001). While there are no major scientific advances relative to the state-of-the-art manifested with this update, documenting the current state of the model and the individual progress that has been made is well appreciated. The paper is generally well written and clear. Nevertheless, I believe there could be more detail given in some of the descriptions to make it a better reference and make the paper more accessible for other modellers. I consequently recommend publication in GMD with some corrections as detailed below.

Thanks for your encouraging comment. We provide a point by point answer to your concern in the following.

General comments:

I believe it is a good practice to (regularly) publish model description papers like the present one, to document the applied models, increase transparency and allow for other modellers to learn, improve upon and critically evaluate the applied techniques. One point I find regrettable with the present paper is that the authors seem to not plan to publish the model code alongside with the manuscript. I know that this may not be common practice in our community, but I believe it would be an important step forward. I would applaud if the authors would think about how to make the code publicly available, possibly with certain restrictions.

We agree with the reviewer on this, however in practice it is not that trivial to make GRISLI code published publicly. The public distribution needs to be done with a specific license (e.g. GNU public licence). Such a license is currently lacking in GRISLI. The model has been developed from the 90ies and has benefited from the additions from numerous contributors. To put a license to the current model, we have to get the permissions to all the contributors from the past 20 years. To date, we do not have this permission from all the contributors. However, as stated in the manuscript, any potential users are encouraged to get in touch with C. Dumas, A. Quiquet or C. Ritz, to start a collaboration.

While the applied modelling techniques are mostly well described in words and equations (textbook style), the numerical implementation is often not possible to determine. I invite the authors to make an additional effort to increase the precision. This is even more important when the model code cannot be consulted. The ultimate goal should be that someone who does not know the model would be able to implement a specific feature from the given information. See also specific points below.

In the revised version of the manuscript, we have expanded on the different subjects: 1) the description of the polynomial flow law and the link between temperature and viscosity; 2) the computation of the flux at the grounding line; 3) the structure of the grids. In addition, we have given more information on the numerical resolution of the equations in the “numerical features” section (Sec. 2.3).

Reference to textbooks and earlier works is mostly in order. However, in some cases it would be useful for the reader to have some additional (’meta’) information for the specific descriptions. E.g. who else is using the same technique, or does the applied technique represent a notable difference/novelty compared to other models used in the community. If other approaches exist, do you have reasons to choose this approach compared to another and why (simplicity, better results,

tried other approach but didn't work ...). Again, the motivation should be to make the paper a useful reference and interesting resource for another modeller trying to implement a specific feature.

Because the novelties were not presented in a sufficiently clear way in the original manuscript, in the revised version, we have systematically referred to the similarities and differences from the previous model description (Ritz et al., 2001). We also have referred to the similarities to other models (SSA velocity as a sliding law, temperature computation, particle tracking scheme, etc.).

Specific comments:

P1 L14 Which time scales or time scale range, be more specific.

From diurnal to multi-millenial. Added in the text.

P1 L15 "surface albedo" is not a feedback, nor "freshwater flux". Please clarify.

Changed for: "[...] through multiple feedbacks such as temperature - surface albedo, gravity waves and oceanic circulation changes related to freshwater flux release."

P1 L18 Not sure about the connection between the two sentences implied here.

Changed for:
"If the two major ice sheets have been mostly stable for at least the last 1000 years, their contribution to global sea level rise in the future is largely uncertain. Conversely, in the past, there is evidence of sea level rise as fast as four metres per century (e.g. Fairbanks, 1989; Hanebuth et al., 2000; Deschamps et al., 2012)."

P1 L21 I would suggest rewording to avoid drastic terms "rapid" and "destabilisation".

We agree with the reviewer that such terms are often used deliberately in inappropriate context. However, our previous sentence directly refers to the melt water pulse 1A event, which leads to abrupt sea level rises as high as 4 m within a century. This event can certainly be qualified as "rapid" and is induced by an ice sheet destabilisation.

P1 L22 "The surface mass balance-height feedback has ..."

Thanks, we have followed your suggestion.

P2 L1-3 Not all bedrock in the Antarctic shows a retrograde slope. More precision needed.

We have added "[…] is related to the fact that large parts of the bedrock presents a retrograde slope [...]"

P2 L4 MISI driven retreat does not have to be very fast. Suggest removing "fast and"

Done.

P2 L7 Add "ice" before "cliff"

Done.

P2 L7 Buttressing already decreases when the ice shelve is removed and a reason for ice cliffs to fail. Reformulate.

True, we have reformulate as follow: “Additional instabilities may also occur on neutral/prograde bed slopes in relation with the structural instabilities of tall ice cliffs (marine ice cliff instability, MICI, Pollard et al., 2015)”

P2 L10 What is the range of temporal and spatial scales, specify.

Changed to:
“Because they include processes operating on variety in temporal, from diurnal to multi-millenial, and spatial scales, from a few metres to thousand of kilometres, [...]”

P2 l10 "temporal and spatial scales" of what exactly?

Now specified, please see our response to your previous comment.

P2 L14 There are also state of the art models that are not FS, clarify.

In this sentence, the term “state of the art” has been replaced by “the most comprehensive”.

P2 L19 Remove "Conversely".

Done.

P2 L21 add "e.g." before Hindmarsh

Done.

P2 L23 Reformulate "temperature and surface mass balance perturbations diffusion"

We removed the word “diffusion”.

P2 L26 New sentence with "GRISLI was in the late nineties ..."

We have done so, thanks for the suggestion.

P3 L4 Not only MISI, but also GL movement in general. Reformulate.

We agree and simply replaced MISI by grounding line migration.

P3 L15 "2.1 Ice thermo-mechanics". I didn't find the "thermo" aspect in this section. Reword?

Section 2.1.6 deals with the temperature computation in GRISLI and the viscosity presented in Sec. 2.1.1 is temperature dependent. The expression of B_AT (and its temperature dependency) is now presented.

P3 L21 Add equation number after "mass conservation equation".

Added.

P3 L23 "the vertically integrated velocities in x and y-direction u_x and u_y".

Done.

P4 L1 "where sigma ... and tau ... are the longitudinal and shearing stress tensor terms, respectively".

It has been changed to:
"[…] where tau_ij=x,y,z are the shearing stress tensor terms and sigma_i=x,y,z the longitudinal stress tensor terms, defined as (i=x,y,z):
sigma_i = tau_ii"

P4 15 Add an equation, explanation or reference how B_AT is calculated.

We acknowledge that this information was missing in the original paper. We have added its equation.

P4 L27-28 SIA and SSA are not yet defined.

This part has been re-written.

P5 L5 "horizontal derivatives" and "vertical derivatives" of what? Clarify.

Of velocity, information added.

P6 L16 How is the water pressure defined? Add equation or reference.

The hydrology model presentation has been largely expanded, including water pressure definition.

*P6 L25 So "beta = C*N" for temperate ice. What is assumed for the rest? Clarify.*

As mentioned in P5L26 of the original manuscript, for cold-based points we imposed a large basal drag that ensures no-slip condition. In addition, sliding velocities are set to 0 in this case. We have added this last precision in the manuscript:
"For cold-based grounded ice we impose a large enough basal drag (typically 10^5 Pa) to ensure virtually no-slip conditions on the bedrock and the basal velocity is set to zero in this case."

P6 L25 I expected to get some information on how C_f is calibrated in this paragraph, maybe just a list of options that could be used, then you get back to that later.

At the end of the paragraph we have added:
"The Cf parameter will be part of the calibrated parameters in our large ensemble."

P6 L29 Avoid use of "flux correction" as it has a specific meaning in coupling climate models. Use e.g. "flux calculation" as on top of the next page.

Done.

P7 L18-19 Here it would be good to already know how the grid is laid out. Where is the velocity defined compared to the ice thickness nodes. You later state that you are using a "staggered Arakawa C-grid", but it may not be clear to all what that implies. Could you add a clear description or figure where the different quantities are defined? This would also help in the following to explain the numerical implementation of certain schemes.

We have added a figure presenting the horizontal staggered grids (Fig. 2), with a description of where the variables are calculated.

P7 L19. So the flux is imposed on two grid points in both x and y direction and applied there simultaneously? More precision is needed to make clear how to implement this.

We acknowledge that the description of the flux computation at the grounding line was somehow incomplete in its description. Relying on the new Fig. 2, we have explained better how the flux computed at the sub-grid position is affecting the actual velocity nodes. This now reads:
“In GRISLI, from the last grounded point in the direction of the flow, we compute the subgrid position of the grounding line in the x and y directions linearly interpolating the floatation criterion (dark green dots in Fig. 2). From this position, the flux at the grounding line is calculated using Eq. 17 or Eq. 18 (red arrows in Fig. 2). Because the flux at the sub-grid position is perpendicular to the local grounding line, ideally we should project this flux onto the x and y-axis. However, in the model, we assume that the grounding line is always perpendicular to either the x or y-axis (dashed brown line in Fig. 2). Similarly to Fürst (2013), the value of the flux qgl is linearly interpolated to the two closest downstream and upstream velocity grid points (dark blue arrows in Fig. 2) using the two bounding velocity points (light blue arrows in Fig. 2).”

P7 L22 Wouldn’t this give back force at the places where velocities are calculated, not at the GL where it is needed?

Yes, the reviewer is perfectly right here. Unfortunately it is not obvious to infer the back force at the grounding line. For example, Pollard and DeConto (2012) and Pattyn (2017) evaluate the back force using the longitudinal stress at the first downstream point.

P7 L27 Replace "Ice front" by "Iceberg" in front of "calving".

Done.

P8 L1 The section header states "Temperature coupling". There is no description of coupling in this section, only how the temperature is calculated. Maybe change title to "Thermodynamics" or "Ice temperature calculation".

You are right. We have reformulated to “Ice temperature calculation” as suggested.

P8 L2 Could give a sentence of introduction to state that this is the classic way to solve thermodynamics and similar to many other models (references). Or is there anything special here that I have overlooked?

The referee is right here, this equation of advection-diffusion is common to most ice sheet models. The introductory sentence reads:

“Similarly to most large-scale ice sheet models (Winkelmann et al., 2011; Pollard and DeConto, 2012; Pattyn 2017), the temperature in GRISLI is computed by solving the general advection-diffusion equation of temperature: [...]”

P8 L2- Consider to give some indication on how all of this is solved numerically. How are the differential equations discretised? Which numerical schemes are used for advection and diffusion (upwind, second order, Lax)?

We have added this information in Sec. 2.3:
“For the temperature equation (Eq. 19), we solved a 1D advection-diffusion equation for each model grid point. The resolution is performed with an upwind semi-implicit scheme (vertical velocity and heat production at the previous time step is used). The ice thermal conductivity is computed as the geometric mean of the two neighbouring conductivity (Patankar, 1980). Because the horizontal diffusion is neglected, the only horizontal terms concern horizontal advection and are computed with an upwind explicit scheme. The heat production is computed at the velocity (staggered) grid points and is then summed up to the temperature (centred) grid points.”

P10 L12 Hardly any information is shared on how the given equations are solved numerically. I believe it would make the paper a much more interesting reference for other modellers and even people in your own group if some details would be added on the practical side of the modelling.

In the revised version, we now explicitly show the staggered grid in Fig. 2. We have also added two additional figures in the supplementary material showing: i) the boundary conditions when extending the front to the edges of the geographical domain and ii) the matrix used to solve the elliptic equation. We have also considerably expanded Sec. 2.3, adding more information on the numerical resolution of the equations:

“The mass balance equation is solved as an advection-only equation with an upwind scheme in space and a semi-implicit scheme in time (velocities at the previous time step are used). The numerical resolution is performed with a point-relaxation method with a variable time step. The value of this time step is chosen to ensure that the matrix becomes strongly diagonal dominant to achieve convergence of the point-relaxation method. The criteria is thus a threshold that is inversely proportional to the fastest velocity on the whole grid. Note that this smaller time step is solely used for the mass conservation equation and subsequent variables (e.g. surface slopes, SIA velocity) while the rest of the model uses a main time step, typically ranging from 0.5 to 5 years depending on the horizontal resolution.

To solve it, the ice shelves/ice streams equation (Eq. 14) is linearised. The viscosity is computed using an iterative method starting from the viscosity calculated from strain rates from the previous time step. As this equation is the most expensive part of the model, the iteration mode is not always used depending on the type of experiment (for instance not crucial when the objective is to reach the steady state). In this case the viscosity of the previous time step is used. The linear system is solved with a direct method (Gaussian elimination, sgbsv in the Lapack library (www.netlib.org/lapack)).”

P10 L13 More precision is needed to understand what variables are defined where on which (staggered) grid, also in the vertical. How is the vertical grid laid out? Is the order up-down or down-up? Is the first vertical grid point from the top where T is solved assumed at the boundary or representing the middle of a first layer? How is that at the base?

We have added a figure that presents a schematic representation of the horizontal staggered grids used in the model (Fig. 2). The direction of the vertical axis z is shown in Fig. 1 (pointing upward). In addition, we have added this information in the section on the numerical features:
“The model uses finite differences computed on a staggered Arakawa C-grid in the horizontal plane (Fig. 2). In the vertical, the model defines σ-reduced coordinates, $\varsigma=(S-z)/H$, for 21 evenly spaced vertical layers, with the z vertical axis pointing upward and ς downward (0 at the surface and 1 at the bottom). The coordinate triplet (i,j,k) (in x, y and ς direction) is representative of the centre of the grid cell.”
The first vertical layer ($\varsigma=0$) has its temperature in equilibrium with the annual mean surface air temperature (Dirichlet boundary condition). In turn, the last vertical layer ($\varsigma=1$) is either at the melting point (Dirichlet boundary condition) or receives heat from the bedrock below (Neumann boundary condition at the bottom of the grid cell).

*P10 L17 "the resolution is *reduced* to ...".*

Right, corrected.

P10 L19 Replace "computes" by "uses" or "computes with". Add "which is dynamically calculated" after "(Eq.2)" or similar.

We have followed your suggestions.

P10 L24-29 Could this be visualised for clarity?

A schematic representation of the matrix is shown in Fig. S1 in the supplementary material.

P10 L28 How small is "small" in this context? Clarify

We have a threshold on the integrated viscosity. Points tagged as “ghost” (see Sec. 3.2) have an integrated viscosity lower than 1500 Pa s. This paragraph has been reformulated.

P11 L1 Add a reference for OpenMP.

We provide an url redirecting to the OpenMP website.

P11 L15 Add a short overview what is coming next before going into details.

We have added at the very beginning of this section:
“In the following, we present a simple calibration methodology for the Antarctic ice sheet based on a large ensemble of model simulations.”

P11 L20 Add reference for ISMIP6 initMIP-Antarctica (ISMIP6 paper, website).

Added reference to Nowicki et al., 2016.

P12 L6 Is K0 changing the basal drag, or the basal drag coefficient? Clarify.

The basal drag coefficient. We now refer more explicitly to variable names and equation numbers presented in Sec. 2.

P12 L10 How does the BMB field keep the ice shelves stable? Clarify.

For ISMIP6 initMIP-Antarctica, we use a data assimilation technique in which the basal drag coefficient is tuned to simulate an ice thickness as close as possible to observations assuming a fixed grounding line position. For ice shelves, we also inverse the basal melting rates under floating ice shelves so that the local (Eulerian) ice thickness derivative is minimal. The inferred basal melting rates are then averaged over the 18 ice shelf domains provided by the InitMIP project. With only a small addition, the sentence has been moved when first showing the present-day sub-shelf basal melting rates:
"Their values are based on the sectoral average of sub-shelf melt rates that ensured stable ice shelves (minimal Eulerian ice thickness derivative) in the recent intercomparison exercise InitMIP-Antarctica (Nowicki et al., 2016), with slight modifications due to change in resolution. They are in line with observations-based estimates (Rignot et al, 2013)."

*P12 L15 In my mind, the basic idea of LHS is to *sample* the hypercube and not perform all possible experiments. Maybe reword to avoid "the whole cube" if this is correct.*

It has been replaced to:
"We perform two times the 300 member ensemble with the flux at the grounding line of [...]".

P12 L19 How is the low resolution data set produced from the original Bedmap2 data? Direct subsampling or smooth interpolation? This is a crucial part of preparing the input data and should be treated with detail and precision.

We simply use a spatial bi-linear interpolation to generate the 40 km input data from the original high-resolution Bedmap2 data. This information has been added in the manuscript. We acknowledge the fact that this can alter the quality of the original data. In particular the shape (direction and slope) of fine scale structures such as narrow valleys and fjords might not be preserved. As stated in the discussion (second paragraph), we aim at introducing some sub-grid information in the model but this has yet to be done.

P12 L20 Reword "discarded from the ensemble" to "not explored in this ensemble"

Thanks for the suggestion, we have followed your suggestion.

P13 L12 If differences are below 500, why does the scale go to 1000 in the figures?

As stated in the manuscript, the differences are *generally* below 500 m although locally (e.g. Ronnie-Filchner area) we could have much larger differences.

P13 L18 Do all these models use the same data, the same processing to get to the final input data and have similar resolution? Do you know if this is an error in the data or a problem of coarse resolution? What is different in models that do not show these features, if there are any?

Pollard and DeConto (2009) also use a 40-km grid, while Martin et al. (2011) use their model at about 20 km resolution. However, input data, notably bedrock elevation / ice thickness and climate forcing, differ and can not explain why different models present systematic biases at the same locations.

The Ronnie-Filchner area presents a complex bedrock topography with pinning points stabilising the grounding line position. The fact that large scale ice sheet models do not explicitly account for sub-grid pinning points can explain consistent biases amongst the models. Similarly, the Transantarctic mountains present narrow ice streams draining part of the East Antarctic ice sheet and are generally poorly represented in large-scale ice sheet models.

More recent publications generally use an inverse method so that ice thickness mismatch with observations is greatly reduced and cannot be directly compared to the results presented in our manuscript.

P13 L20 If the last point is resolved, maybe "... suggesting a common source of error related to the coarse model resolution". Or similar to add some interpretation to this comparison.

We have added the following:
“Consistent model biases amongst these models, which use different input data, suggest a common source of error related to the coarse model resolution (20 to 40 km) or uncertainties in the bedrock dataset, particularly large in East Antarctica (Fretwell et al., 2013).”

P16 L3 How can you be sure that the parameter range is sufficient/optimal for the transient experiments? Please add a short discussion on that.

For the transient experiments, we used the twelve ensemble members that show the lowest RMSE when forced by perpetual present-day SMB. This shows the simulated variability through glacial-interglacial cycles for models calibrated on present-day ice sheet geometry. This is of course a too small subset to properly address the inter-model differences but we believe it is sufficient to discuss the general variability because the models produce similar evolutions. Ideally, we would have run all the ensemble members with the transient forcing and only kept the members showing the lowest RMSE at 0 kaBP. However, uncertainties in the climate forcing will also have biased the model responses.

We have nonetheless moderated the sentences:
“The uncertainty related to the choice of the internal parameters within our subset leads generally to up to [...]”

P16 L10 Maybe "post-LGM retreat"?

Thanks for the suggestion. Added.

P17 L4 "relative to observations ... in this case, where ..." and briefly remind us what is different in the present experiments.

This now reads:
“Whilst the model is able to reproduce present-day Greenland (Le clec’h et al., 2017) and Antarctic (Ritz et al., 2015) ice sheets when using an inverse method to estimate the basal drag, our simulations with an interactive basal drag computed from the effective pressure show some important disagreements relative to observations.”

P17 L5 Where is the northern part of East Antarctica? polewards = south!, north=towards the margin?

We have reformulated as:
“In particular there are some persisting model biases in ice thickness. In East Antarctica, the ice thickness is underestimated towards the pole and the Transantarctic mountains while it is overestimated towards the margins, from Queen Maud land to Wilkes land. In West Antarctica, there is an underestimation of ice thickness in the Ronnie-Filchner basin and an overestimation in the Ross basin.”

P17 L15 Inversion of what? Specify.

Changed to:
“However, by design, the fit with observations is systematically poorer compared to model results that make use of an inverse basal drag coefficient.”

P17 L23 This comes a bit unexpected. Has vertical temperature been worked on in this paper? Why only the vertical?

For sake of clarity, we have been more specific in the introductory sentence:
“Although widely used for ice sheet model spin-up or calibration, long-term integrations under present-day forcing induce a warm bias in the vertical temperature profile because they discard the diffusion of glacial-interglacial changes in surface temperature.”

In our paper, the calibration step has been done assuming a perpetual present-day climate forcing, which necessarily bias our simulated temperature field towards too high value. We believe that this point deserves discussion in this section and we have kept it in the revised manuscript.

P17 L33 "lead to a more dynamic grounding line position"

We have followed your suggestion.

P17 L34 Has sensitivity to SL changes really been discussed in the paper?

We have not tested explicitly the sensitivity to sea level change in this paper but it has been accounted for when performing glacial-interglacial simulations.

P17 L34 Add sensitivity to sub-shelf melt rates?

We now mention the sub-shelf melt rates. However, our point here was about changes in sea level and its local variations as this has been relatively unexplored within large-scale ice sheet model while sub-shelf melt rates is known to be a driver for glacial-interglacial Antarctic variability.

P18 L11 Basal hydrology and semi-lagrangian tracking are described in "2.2 Additional features" next to other aspects that are not mentioned here in the conclusions. It may be useful to make it clearer already in the main text which of the described features are new developments in GRISLI.

The “additional features” section contains material that is not directly related to the ice model itself (ice sheet thermo-mechanics). In this section, there is indeed old and new model features.

The basal hydrology has only been documented in a Phd dissertation written in French (Peyaud, 2006). The semi-lagrangian tracking has been presented by Lhomme et al. (2005) but for an other

ice sheet model. It has been re-implemented in GRISLI for Quiquet et al. (2013) but has not been described there.

In the revised version of the manuscript we have listed better the difference with Ritz et al. (2001). Following is a list of the additions in the revised manuscript:

Introduction
"We also provide details on some components (sub-glacial hydrology and tracking particle scheme embedded in GRISLI) which are currently not documented in international scientific journals."

Section 2.1.1
"Ice deformation and mass conservation in GRISLI version 2.0 is mostly treated as in Ritz et al. (2001) with the notable exception of the use of a polynomial flow law with the introduction of a linear, Newtonian, viscosity."

Section 2.1.2
"Differing from Ritz et al. (2001), the velocity in GRISLI is now computed for the entire domain as the superposition of the shallow ice approximation (SIA) and the shallow shelf approximation (SSA) components, without using a sliding law to estimate basal velocities."

Section 2.1.6
"The ice temperature calculation has remained identical to Ritz et al. (2001)."

Section 2.2.1
"In the following we provide a complete description of the hydrology model because it has only been described in a French Phd dissertation (Peyaud, 2006) but currently lacks a description in an international scientific journal."

Section 2.2.2
"As in Ritz et al. (2001), GRISLI computes the bedrock response to ice load with an [...]".

Section 2.2.3
"GRISLI includes a passive tracer model that allows for the computation of vertical ice stratigraphy, i.e. time and location of ice deposition for the vertical model grid points. The model is the one of Lhomme et al. (2005) re-implemented in GRISLI by Quiquet et al. (2013)."

P18 L26 Why does validating a model for the Antarctic give confidence to also use it for the NH. A bit more information is needed here to bridge that gap.

If we consider today ice sheets that are still present now, the Antarctic ice sheet is a good case study because of its interaction with the ocean which could have been more important through glacial-interglacial cycles compared to the Greenland ice sheet. The fact that we manage to reproduce the Antarctic ice sheet variability gives some confidence in the ability of the model to simulate large grounding line migration that could have happened for palaeo ice sheets such as for example the Kara-Barents ice sheet. However, sub-glacial conditions (e.g. till distribution and rheology) are probably largely different and this has not been explored in the present manuscript. To avoid overstated statement we have decided to remove this sentence from the revised manuscript.

P18 L30 Replace "and" by "or", unless all three have to be contacted to get the model code.

Changed to “or”, no need to contact all three.

Tables and figures

P26 in the middle. Replace "N.m" by "N m"?

Yes, changed.

P27 caption Table 2. Write out LHS.

Done.

P27 Figure 2. Left panel cold have additional contours to delineate the regions and a colour bar. Why does the grounding line have different melting rates than the shelf?

The left panel simply displays the different sectors as defined in ISMIP6 InitMIP-Antarctica (Nowicki et al., 2016). The numbering is irrelevant as we never refer to the sector number in the text. We have nonetheless changed the color coding so as to show better the extent of the different sectors.

We have added this in the figure caption:
“The melting rates are different for the shelf and the associated grounding line to mimic the higher values observed close to the grounding line Rignot et al. (2013).”

P29 Figure 5. Use a colour for the GL contour that does not appear in the colour map, e.g. black or dark gray.

Thanks for the suggestion, we have used dark grey instead of red.

P30 Figure 6. Same as for figure 5.

Changed here as well.

P32 Figure 8. Suggest to move the parameter values to a table or the main text.

We have moved this information to a table.

P34 Figure 12. "materialised" –> "shown" or "indicated" Why is the GL so patchy here compared to the steady state case?

We have chosen the word “indicated”.

Fig. 5 and Fig. 6 in the original manuscript shows only the present-day observed grounding line. But in fact the grounding line is also relatively patchy for the steady state as soon as the model simulates a significant departure from present-day position. You will find below the surface elevation for the two ensemble members that show the lowest RMSE in Sec. 3 (100-kyr simulation under perpetual climate) in which the grounding line is indicated by a thick red line.

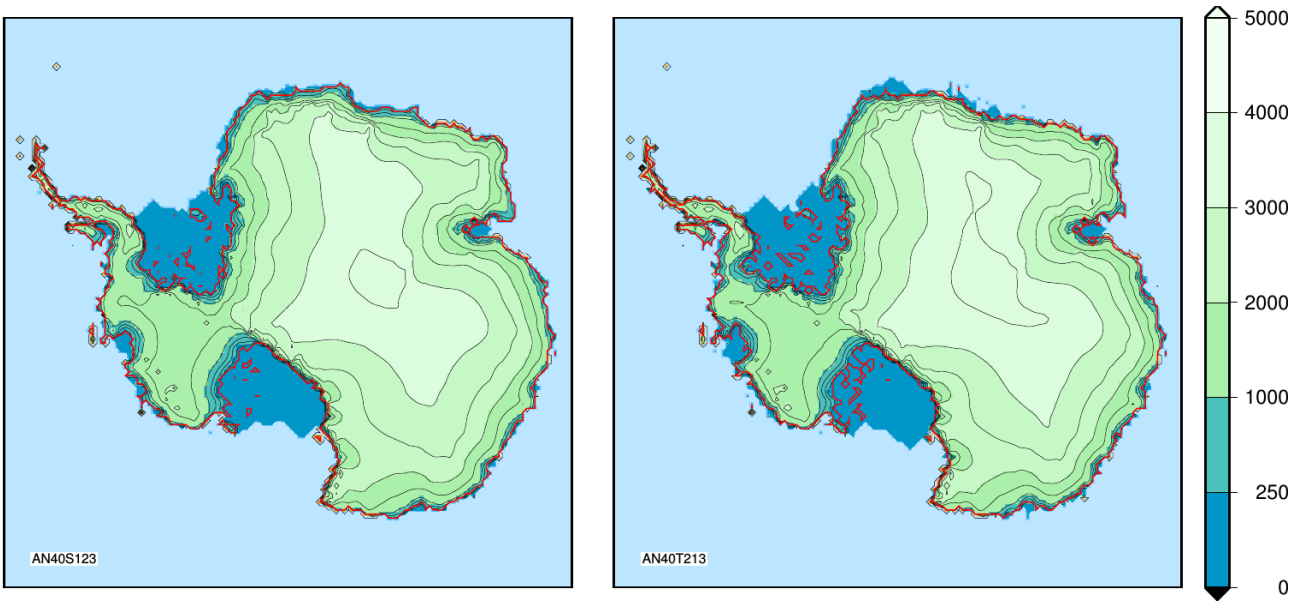

Figure R1: Simulated surface elevation at the end of the 100 kyrs simulations forced by perpetual present-day climate (Sec. 3) for the two ensemble members that show the lowest RMSE with respect to the observations (AN40S123 and AN40T213). The grounding line is indicated by the thick red line.

P35 Figure 13. Same as for figure 5.

Changed here as well.

The GRISLI ice sheet model (version 2.0): calibration and validation for multi-millennial changes of the Antarctic ice sheet

Aurélien Quiquet[1], Christophe Dumas[1], Catherine Ritz[2], Vincent Peyaud[2], and Didier M. Roche[1,3]

[1]Laboratoire des Sciences du Climat et de l'Environnement (LSCE), UMR8212, CEA/CNRS-INSU/UVSQ, Gif-sur-Yvette Cedex, France

[2]Université Grenoble Alpes, CNRS, IRD, IGE, F-38000 Grenoble, France

[3]Earth and Climate Cluster, Faculty of Science, Vrije Universiteit Amsterdam, Amsterdam, the Netherlands

Correspondence to: A. Quiquet (aurelien.quiquet@lsce.ipsl.fr)

Abstract.

In this paper we present the GRISLI (Grenoble Ice Sheet and Land Ice) model in its newest revision (version 2.0). Whilst GRISLI is applicable to any given geometry, we focus here on the Antarctic ice sheet because it highlights the importance of grounding line dynamics. Important improvements have been implemented since its original version (Ritz et al., 2001) including notably an explicit flux computation at the grounding line based on the analytical formulations of Schoof (2007) ~~and~~ or Tsai et al. (2015) and a basal hydrology model. A calibration of the mechanical parameters of the model based on an ensemble of ~~150~~ 300 members sampled with a Latin Hypercube method is used. The ensemble members performance is assessed relative to the deviation from present-day observed Antarctic ice thickness. The model being designed for multi-millenial long-term integrations, we also present glacial-interglacial ice sheet changes throughout the last 400 kyr using the best ensemble members. To achieve this goal, we construct a simple climatic perturbation of present-day climate forcing fields based on two climate proxies, both atmospheric and oceanic. The model is able to reproduce expected grounding line advances during glacials and subsequent retreats during terminations with reasonable glacial-interglacial ice volume changes.

1 Introduction

Continental ice sheets are a major component for the Earth system dynamics operating on a variety of timescales, from diurnal to multi-millenial, through multiple feedbacks such as temperature - surface albedo, gravity waves and ~~freshwater flux to the ocean~~oceanic circulation changes related to freshwater flux release. Over the last decades, modern observation techniques of the Greenland and Antarctic ice sheets (e.g. altimetry, gravimetry, echo sounding) have shown important changes such as an increase in surface and sub-shelf melt, glacier speed-up, dynamical thinning and drastic calving events (e.g. Mouginot et al., 2015; Paolo et al., 2015; Hall et al., 2013; Pritchard et al., 2009). ~~Whilst the contribution of these ice sheets~~ If the two major ice sheets have been mostly stable for at least the last 1000 years, their contribution to global sea level rise in the future is largely uncertain~~, there are evidences~~. Conversely, in the past, there is evidence of sea level rise as fast as four metres per century ~~in the past~~ (e.g. Fairbanks, 1989; Hanebuth et al., 2000; Deschamps et al., 2012). The study of well-recorded past events can help us to constrain the fate of the ice sheets in a warming Earth and to disentangle the role of the different processes leading to

rapid ice sheet destabilisation. The surface ~~elevation feedback on ice sheet surface mass balance~~ mass balance-height feedback has often been proposed as a major driver for rapid northern Hemisphere ice sheets disintegration (e.g. Abe-Ouchi et al., 2013; Gregoire et al., 2012). ~~An other~~ Another source of instability, for marine ice sheets such as the palaeo Kara-Barents or present-day Antarctic ice sheets, is related to the fact that large parts of the bedrock presents a retrograde slope from the grounding line and deepens well below sea level due, for instance, to isostatic adjustment or within glacial troughs. Such properties lead to the marine ice sheet instability (MISI, Weertman, 1974; Schoof, 2007) responsible for ~~a fast and~~ an irreversible retreat of the grounding line in response to an initial perturbation such as local sea level change and/or increase in basal melting rate below ice shelves. Such processes are expected to play a crucial role for the stability of the Antarctic ice sheet in the future (e.g. Favier et al., 2014). Additional instabilities may also occur on neutral/prograde bed slopes ~~and have been attributed to cliff instabilities and the associated decrease in ice-shelf buttressing~~ in relation with the structural instabilities of tall ice cliffs (marine ice cliff instability, MICI, Pollard et al., 2015).

Because ~~of the~~ they include processes operating on variety in temporal, from diurnal to multi-millenial, and spatial scales, from a few metres to thousand of kilometres, but also due to the lack of crucial observations (e.g. basal conditions and internal thermo-mechanics), continental ice sheets are difficult to model. Most numerical models consider ice sheets as an incompressible fluid, where motion can be described with the Navier-Stokes equations. Even if some processes have generally to be parameterised (e.g. ice anisotropy), the complete set of equations can be solved explicitly and does not require the use of any approximation. ~~State of the art~~ The most comprehensive continental ice sheet models, namely the Full-Stokes models, solve explicitly all the terms in the stress tensor (Gillet-Chaulet et al., 2012; Larour et al., 2012). Recent applications are promising but, due to computational cost, continental scale applications are currently limited to a few centuries. As such, they are not yet the ~~right~~ most suitable tool for palaeo-reconstructions or multi-millenial future projections.

~~Conversely, in~~ In order to decrease the degree of complexity, simpler models were historically developed that make use of the small aspect ratio of ice sheets (vertical to horizontal scale ratio) to derive approximations for the Navier-Stokes equations ~~(Hindmarsh, 2004)~~(e.g. Hindmarsh, 2004). Such models present the advantage to be much cheaper compared to Full-Stokes models, allowing for multi-millenial integrations. They are well-suited to study slow feedbacks such as glacio-isostasy or the impact of temperature and surface mass balance perturbations~~diffusion~~. The Grenoble ice sheet and land ice (GRISLI) model belongs to the latter category (Ritz et al., 2001). GRISLI consists of the combination of the inland ice model of Ritz (1992) & Ritz et al. (1997) and the ice shelf model of Rommelaere and Ritz (1996), extended to the case of ice streams treated as *dragging ice shelves*~~, GRISLI being at that time~~ . GRISLI was in the late nineties the first large scale ice sheet model with an hybrid shallow ice / shallow shelf system of equations. Whilst since Ritz et al. (2001) the fundamental equations for ice dynamics have not drastically changed, the model has nonetheless benefited from the numerous works which used it. To date, 30 papers published or in peer-review discuss GRISLI model simulation results. The range of applications have been very wide ranging from ice sheet reconstructions for deep-time palaeo-climate (e.g. Benn et al., 2015; Donnadieu et al., 2011; Ladant et al., 2014) and Quaternary (e.g. Peyaud et al., 2007; Alvarez-Solas et al., 2013; Quiquet et al., 2013; Colleoni et al., 2016) to

future sea level rise projections (e.g. Ritz et al., 2015; Peano et al., 2017). GRISLI has participated in several inter-comparison exercises (Calov et al., 2010; Edwards et al., 2014; Koenig et al., 2015; Goelzer et al., 2017) and has been coupled to climate models of various complexities (e.g. Philippon et al., 2006; Roche et al., 2014; Le clec'h et al., 2018).

The aim of our current study is to provide a technical description of the GRISLI model in its current version (GRISLI version 2.0, hereafter GRISLI), including the several additional features from Ritz et al. (2001). In particular, we have now included an explicit flux computation at the grounding line following the analytical formulation from Schoof (2007) and Tsai et al. (2015) in order to have a better representation of the ~~MISI~~grounding line migration. We also provide details on some components (sub-glacial hydrology and tracking particle scheme embedded in GRISLI) which are currently not documented in international scientific journals. In addition, we present a simple calibration of the mechanical parameters suitable for multi-millenia integrations and we show an example of the model response to glacial-interglacial forcing.

In Sec. 2 we describe the fundamental equations of the GRISLI ice sheet model with a particular emphasis on the model developments departing from Ritz et al. (2001). In sec. 3, we present a simple calibration methodology which aims at reproducing the observed present-day Antarctic ice sheet geometry. In Sec. 4, we discuss the ability of the model to simulate the Antarctic ice sheet changes over the last four glacial-interglacial cycles.

2 The GRISLI ice sheet model

GRISLI constitutive equations were presented in Ritz et al. (2001) and we aim here at giving a broad comprehensive description of the current model version, with its latest functionalities. Major model parameters are listed in Tab. 1.

2.1 Ice thermo-mechanics

2.1.1 Ice deformation and mass conservation

Ice deformation and mass conservation in GRISLI version 2.0 is mostly treated as in Ritz et al. (2001) with the notable exception of the use of a polynomial flow law with the introduction of a linear, Newtonian, viscosity.

GRISLI considers the ice sheet as solely formed of pure ice with a constant and homogeneous density (ρ_{ice} ~~ρ~~). In this approximation, the ice being considered as an incompressible fluid, the mass conservation equation can be written as:

$$\nabla.\mathbf{u} = \frac{\partial u_x}{\partial x} + \frac{\partial u_y}{\partial y} + \frac{\partial u_z}{\partial z} = 0 \tag{1}$$

with (u_x, u_y, u_z) the Cartesian components of the ice velocity field.

The vertically integrated expression of the mass conservation equation (Eq. 1) provides the equation for the ice thickness, H:

$$\frac{\partial H}{\partial t} = -\frac{\partial H\bar{u_x}}{\partial x}\frac{\partial H\bar{u}_x}{\partial x} - \frac{\partial H\bar{u_y}}{\partial y}\frac{\partial H\bar{u}_y}{\partial y} + M - b_{melt} \tag{2}$$

with ~~$\bar{u}_x$ and $\bar{u}_y$~~ $\bar{u}_x$ and $\bar{u}_y$ the vertically integrated velocities in x and y~~velocities~~-directions, M the surface mass balance and b_{melt} is the basal melting rate.

The quasi-static approximation is used for the velocity field, in which the inertial terms of the momentum conservation equation are ignored. The gravity force being the sole external force acting on an infinitesimal cube of ice, we have:

$$\begin{cases} \frac{\partial \sigma_x}{\partial x} + \frac{\partial \tau_{xy}}{\partial y} + \frac{\partial \tau_{xz}}{\partial z} = 0 \\ \frac{\partial \tau_{xy}}{\partial x} + \frac{\partial \sigma_y}{\partial y} + \frac{\partial \tau_{yz}}{\partial z} = 0 \\ \frac{\partial \tau_{xz}}{\partial x} + \frac{\partial \tau_{yz}}{\partial y} + \frac{\partial \sigma_z}{\partial z} = \rho_i g \end{cases}$$

~~where $\sigma_{i=x,y,z}$, respectively~~

$$\begin{cases} \frac{\partial \sigma_x}{\partial x} + \frac{\partial \tau_{xy}}{\partial y} + \frac{\partial \tau_{xz}}{\partial z} = 0 \\ \frac{\partial \tau_{xy}}{\partial x} + \frac{\partial \sigma_y}{\partial y} + \frac{\partial \tau_{yz}}{\partial z} = 0 \\ \frac{\partial \tau_{xz}}{\partial x} + \frac{\partial \tau_{yz}}{\partial y} + \frac{\partial \sigma_z}{\partial z} = \rho g \end{cases} \quad (3)$$

where $\tau_{ij=x,y,z}$ ~~, are the longitudinal, respectively shearing ,~~ are the shearing stress tensor terms ~~.~~ and $\sigma_{i=x,y,z}$ the longitudinal stress tensor terms, defined as ($i = x, y, z$):

$$\sigma_i = \tau_{ii} \quad (4)$$

The pressure is defined as the first invariant of the stress tensor:

$$-P = \frac{\sigma_x + \sigma_y + \sigma_z}{3} \quad (5)$$

The deviatoric stress tensor is defined as (for $i, j = x, y, z$):

$$\tau'_{ij} = \tau_{ij} + \delta_{ij} P \quad (6)$$

with δ_{ij} being 1 for $i = j$, 0 otherwise.

Assuming isotropy, the deviatoric stress and the deformation rate $\dot{\epsilon_{ij}}$ are related by:

$$\tau'_{ij} = 2\eta \dot{\varepsilon_{ij}} \quad (7)$$

where η is the ice viscosity.

~~Alike~~ Like most ice sheet models, GRISLI considers the ice as a non-Newtonian viscous fluid following a Norton-Hoff constitutive law (commonly named Glen flow law):

$$\frac{1}{\eta} = B_{AT} \tau^{n-1} \quad (8)$$

where B_{AT} is a temperature-dependent coefficient ~~following an Arrhenius law,~~ and τ is the effective shear stress, defined as (for $i = x, y, z$):

$$\tau^2 = \frac{1}{2} \sum_{i,j} \tau_{ij}^2 \tag{9}$$

The temperature-dependant coefficient B_{AT} is computed with an Arrhenius law:

$$B_{AT} = S_f B_{BAT0} \exp\left(\frac{E_a}{R}\left(\frac{1}{T_m} - \frac{1}{T}\right)\right) \tag{10}$$

where S_f is a flow enhancement factor, B_{BAT0} is a flow law coefficient, E_a is the activation energy, R the gas constant, T_m the ice pressure melting temperature and T the local temperature.

To account for the fact that the activation energy increases close to the melting point (Le Gac, 1980), in GRISLI, the pair (E_a, B_{BAT0}) can take two different values for local temperatures higher or lower than a temperature threshold T^{trans} (Tab. 1).

The Glen flow law is an empirical formulation, derived from laboratory experiments. However, laboratory experiments fail at reproducing the range of deviatoric stress values expected in real ice sheets. The timescale over which this stress is applied in real ice sheets is also not reproducible in laboratories. If most modelling studies agree to use $n = 3$ for the Glen flow law exponent (Eq. 8), there is room for uncertainties as a few studies suggest the possibility for a smaller exponent for small stress regime (Duval and Lliboutry, 1985; Pimienta, 1987; Pettit and Waddington, 2003). ~~One~~ Since the work of Dumas (2002), one particularity of GRISLI is the possibility to simultaneously use a Glen viscosity with $n = 3$ and a linear, Newtonian, viscosity with $n = 1$~~(Dumas, 2002)~~. In this case, the two contributions simply add up:

$$2\,\dot{\varepsilon}_{ij} = \left(B_{AT1} + \tau^2 B_{AT3}\right)\,\tau'_{ij} \tag{11}$$

~~Alike~~ with B_{AT1} and B_{AT3} computed with Eq. 10, only using different activation energy ($E_{a\,1}$ and $E_{a\,3}$), flow law coefficient ($B_{BAT0\,1}$ and $B_{BAT\,3}$) and temperature threshold (T_1^{trans} and T_3^{trans}). The chosen values (Tab. 1) are based on Lipenkov et al. (1997).

Like other large scale ice sheet models, GRISLI does not take into account explicitly anisotropy~~. Anisotropy~~ , which tends to facilitate deformation due to vertical shear~~(i.e. in the slow flowing regions, treated with the SIA)~~, but reduces ~~the~~ deformation due to longitudinal stress~~(i. e. in the fast flowing regions, treated with the SSA regions). In GRISLI, a~~ . The role of the flow enhancement factor ~~is applied in the Glen equation used in the SIA (S_f in Eq. 8) to favour longitudinal deformations. At the same time,~~ 10 is to artificially account for the effect of anisotropy. S_f takes different values for the two components of the velocities computed in GRISLI (due to vertical shearing or longitudinal deformation, presented in the next section). In particular, we use a fixed ratio~~between the SIA and SSA enhancement factor is used~~, typically ranging from 5:1 to 10:1 ~~, as suggested by Ma et al. (2010)~~(Ma et al., 2010), between the value of the enhancement factor S_f for vertical shear and the one for longitudinal deformation. In the following, this ratio will be set to 8:1 and the enhancement factor S_f for vertical shearing with a Glen viscosity will be part of the calibrated parameters. In turn, the flow enhancement factor for the vertical shearing with a linear viscosity is set to 1.

2.1.2 Ice velocity

~~The~~ Differing from Ritz et al. (2001), the velocity in GRISLI is now computed for the entire domain as the superposition of the shallow ice approximation (SIA) and the shallow shelf approximation (SSA) components, without using a sliding law to estimate basal velocities.

The SIA (Hutter, 1982) assumes that the horizontal derivatives of velocity are much smaller than ~~the~~ its vertical derivatives, which is generally true for the major part of the ice sheet where the gravity driven flow induces a slow motion of the ice. GRISLI uses the zero order of the SIA approximation in which the stress tensor components simplified to:

$$\begin{cases} \tau_{xz} = \rho g \dfrac{\partial S}{\partial x}(S-z) \\ \\ \tau_{yz} = \rho g \dfrac{\partial S}{\partial y}(S-z) \end{cases} \tag{12}$$

with S the surface elevation. The vertical velocity profile is computed as an integral from the bedrock ~~(for $i = x, y, z$~~elevation, B, to a given vertical coordinate, z (for $i = x, y$):

$$u_i(z) = u_{ib} + \int_B^z 2\,\dot{\varepsilon}_{iz}\,dz \tag{13}$$

where u_{ib} is the i component of the basal velocity.

The basal velocity can be computed with a sliding law (e.g. Bindschadler, 1983). However, recent versions of GRISLI use the shallow shelf approximation (SSA) as a sliding law as suggested by Bueler and Brown (2009). In this case, similarly to Winkelmann et al. (2011) we simply add up the two contributions of the SIA and SSA for the whole domain which ensure a smooth transition from non-sliding frozen regions to sliding over a thawed bed.

For the fast flowing regions the vertical stresses are much smaller than the longitudinal shear stresses. In this case, the velocity fields with the SSA (MacAyeal, 1989) reduced to the following elliptic equations:

$$\begin{cases} \dfrac{\partial}{\partial x}\left(2\bar{\eta}H\,(2\,\dfrac{\partial u_x}{\partial x}+\dfrac{\partial u_y}{\partial y})\right)+\dfrac{\partial}{\partial y}\left(\bar{\eta}H\,(\dfrac{\partial u_x}{\partial y}+\dfrac{\partial u_y}{\partial x})\right)=\rho g H\,\dfrac{\partial S}{\partial x}-\tau_{bx} \\ \\ \dfrac{\partial}{\partial y}\left(2\bar{\eta}H\,(2\,\dfrac{\partial u_y}{\partial y}+\dfrac{\partial u_x}{\partial x})\right)+\dfrac{\partial}{\partial x}\left(\bar{\eta}H\,(\dfrac{\partial u_y}{\partial x}+\dfrac{\partial u_x}{\partial y})\right)=\rho g H\,\dfrac{\partial S}{\partial y}-\tau_{by} \end{cases} \tag{14}$$

where ~~S is the surface topography and~~ τ_b is the basal drag. The velocities u_x and u_y are identical along the vertical dimension.

The condition at the front of the ice shelf is given by the balance between the water pressure and the horizontal longitudinal stress (see also ~~numerical feature)~~Sec. 2.3 on the numerical features).

2.1.3 Basal drag

For floating ice shelves, the basal drag, τ_b, is ~~zero~~neglected. For cold-based grounded ice we impose a large enough basal drag (typically ~~$10^5 Pa$~~10^5Pa) to ensure virtually no-slip conditions on the bedrock and the basal velocity is set to zero in this case. For temperate-based grounded ice, a power-law basal friction (Weertman, 1957) is assumed:

$$\begin{cases} \tau_{bx}^m = -\beta\, u_{bx} \\ \\ \tau_{by}^m = -\beta\, u_{by} \end{cases} \tag{15}$$

where the basal drag coefficient β is positive. In the experiment presented here, we assume the presence of a sediment at the base of the ice sheet allowing for a viscous deformation ($m = 1$).

In some recent applications of GRISLI, the basal drag coefficient has been inferred with an inverse method in order to match present-day ice sheet geometry (Ritz et al., 2015; Le clec'h et al., 2018). This approach has been followed to participate in the first phase of the recent ice sheet model intercomparison project (ISMIP6, Nowicki et al., 2016) for both the Greenland (Goelzer et al., 2017) and Antarctic ice sheets. In this context, GRISLI achieves to provide sea level rise projections by the end of the century in line with the results from more complex model (Edwards et al., 2014; Goelzer et al., 2017).

~~However, inverse~~ Inverse methods are particularly adapted to produce an ice sheet state (e.g. geometry and/or velocity) close to observations. However, such methods do not provide information for grid points that are not glaciated today by construction. As such they are ~~not applicable~~ difficult to apply for palaeo reconstructions of the American or Eurasian ice sheets. More generally, inverse methods are no longer appropriate for long-term integrations, either palaeo or future, when ice thickness is very different from its present state and especially when ice boundary migrates from its present-day position. This motivates the use of a basal drag coefficient depending on GRISLI internal variables. We generally assume that its value is modulated by the effective water pressure, N, at the base of the ice sheet:

$$\beta = C_f N \tag{16}$$

with C_f an internal parameter that needs calibration.

In our approach, any temperate-based grounded point will have a non-zero sliding velocity, depending on the C_f factor used. Previous works have used additional criteria to limit the extension of these ice streams. For example, Alvarez-Solas et al. (2010) only compute Eq. 16 where the present-day sediment thickness exceeds a certain threshold whilst Quiquet et al. (2013) restrict this to large-scale valleys. However these approaches have flaws. For example, the sediment distribution is only poorly known below present-day ice sheets and its past evolution is largely uncertain. Also, the definition of a typical spatial scale for ice streams is somehow arbitrary. For these reasons, in the following we use the simplest approach and compute Eq. 16 for any temperate-based grid point. The C_f parameter will be part of the calibrated parameters in our large ensemble.

2.1.4 Flux at the grounding line

In Ritz et al. (2001) the position of the grounding line was computed from a simple floatation criterion with no ~~additional flux correction~~specific flux computation at the grounding line. Such an approach is in theory only valid for a very high spatial resolution, within tenths of meters, at the vicinity of the grounding line (Durand et al., 2009). Because the model runs typically at a much coarser resolution, in GRISLI version 2.0 we have implemented an explicit flux computation at the grounding line based on the analytical formulations from Schoof (2007) and Tsai et al. (2015). The two formulations differ from the assumption made on the sediment rheology.

The flux at the grounding line following Schoof (2007) is:

$$q_{gl}^{S} = -\left(\frac{\bar{A}(\rho_i g)^{n+1}(1-\rho_i/\rho_w)^n}{4^n\beta}\,\frac{\bar{A}(\rho g)^{n+1}(1-\rho/\rho_w)^n}{4^n\beta}\right)^{\frac{m}{m+1}} H_{gl}^{\frac{m(n+3)+1}{m+1}}\,\phi_{bf}^{\frac{m\,n}{m+1}} \tag{17}$$

with n and m being the exponents in the Glen flow law (Eq. 8) and in the friction law (Eq. 15) respectively, $\bar{A}$ the vertically integrated temperature dependent coefficient in the Glen flow law (B_{AT}, Eq. 8), H_{gl} the ice thickness at the grounding line, and ϕ_{bf} a back force coefficient to take into account the buttressing role of ice shelves. β is the basal drag coefficient presented in Eq. 15.

Conversely, Tsai et al. (2015) proposed:

$$q_{gl}^{T} = Q_0\,\frac{8\bar{A}(\rho_i g)^n}{4^n f}\,\frac{8\bar{A}(\rho g)^n}{4^n f}\left(1-\rho_i/\rho_w\right)^{n-1} H_{gl}^{\,n+2}\,\phi_{bf}^{n-1} \tag{18}$$

with $Q_0 = 0.61$. In this case, the basal drag is assumed to vanish at the grounding and as such the coefficient β is not used. Instead Tsai et al. (2015) suggests a constant and homogeneous basal friction coefficient f set to 0.6.

In GRISLI, from the last grounded point in the direction of the flow, we compute the subgrid position of the grounding line in the x and y directions linearly interpolating the floatation criterion (dark green dots in Fig. 2). From this position, the flux at the grounding line is calculated using Eq. 17 or Eq. 18 ~~. Then~~ (red arrows in Fig. 2). Because the flux at the sub-grid position is perpendicular to the local grounding line, ideally we should project this flux onto the x and y-axis. However, in the model, we assume that the grounding line is always perpendicular to either the x or y-axis (dashed brown line in Fig. 2). Similarly to Fürst (2013), the value of the flux q_{gl} is linearly interpolated to the two closest downstream and upstream velocity grid points ~~similarly to Fürst (2013)~~(dark blue arrows in Fig. 2) using the two bounding velocity points (light blue arrows in Fig. 2).

To evaluate the back force coefficient ϕ_{bf}, we solve the velocity equation twice~~, with and without ice shelves. The ratio in velocity for the grounded ice sheet points provides the back force coefficient ϕ_{bf}. In the model, to inhibit the buttressing role of ice shelves without changes in geometry, they are assigned a very small~~ . The first iteration is computed on the simulated

geometry with no specific flux adjustment at the grounding line (i.e. not using Eq. 17 nor Eq. 18). The second iteration is computed the same way, except for the fact that the ice shelves are assigned to a very low viscosity so that they ~~do not~~ cannot exert any back force. The buttressing ratio ϕ_{bf} is then computed as the velocity ratio between these two computed velocities. Once ϕ_{bf} is estimated, we solve the velocity equation again, this time imposing the grounding line flux computation using Eq. 17 or Eq. 18, in order to estimate the velocity used in the mass conservation for this time step. We acknowledge the fact that this approach is computationally expensive but it allows for more accurate estimate for the buttressing role of ice shelves in the model.

2.1.5 Calving

~~Ice front~~ Iceberg calving is not modelled explicitly. Instead, we used a simple ice thickness threshold criterion. Because this simple scheme can prevent ice shelf extension, we also maintain downstream ice shelf grid-points neighbouring the last grid-points meeting the criterion. The cut-off threshold may vary in space (e.g. oceanic depth dependency) and time. In the following, we use a constant and homogeneous thickness criterion (set to 250 m, roughly corresponding to the observed present-day Antarctic ice shelves front).

2.1.6 ~~Temperature coupling~~Ice temperature calculation

~~Regarding the thermo-mechanical coupling, GRISLI solves~~ The ice temperature calculation has remained identical to Ritz et al. (2001). Similarly to most large-scale ice sheet models (e.g. Winkelmann et al., 2011; Pollard and DeConto, 2012; Pattyn, 2017), the temperature in GRISLI is computed by solving the general advection-diffusion equation of temperature:

$$\frac{\partial T}{\partial t} = \underbrace{\frac{1}{\rho c}\frac{\partial}{\partial x}\left(k_i \frac{\partial T}{\partial x}\right) + \frac{1}{\rho c}\frac{\partial}{\partial y}\left(k_i \frac{\partial T}{\partial y}\right)}_{\text{horizontal diffusion}} \underbrace{+\frac{1}{\rho c}\frac{\partial}{\partial z}\left(k_i \frac{\partial T}{\partial z}\right)}_{\text{vertical diffusion}} \underbrace{-u_x \frac{\partial T}{\partial x} - u_y \frac{\partial T}{\partial y}}_{\text{horizontal advection}} \underbrace{-u_z \frac{\partial T}{\partial z}}_{\text{vertical advection}} \underbrace{+\frac{Q}{\rho c}}_{\text{heat production}} \tag{19}$$

with k_i the thermal conductivity of the ice and c the heat capacity. uz is the vertical velocity, computed as in Ritz et al. (1997) (wt in Eq. 14 of the original paper).

Horizontal diffusion is assumed to be much smaller than the vertical one and is therefore neglected.

The heat production is given by Hutter (1983) (for $i, j = x, y, z$):

$$Q = \sum_{i,j} \dot{\varepsilon}_{ij} \tau_{ij} \tag{20}$$

At the ice sheet surface, due to the absence of an explicit snowpack model, ice temperature is assumed to be equal to the near-surface air annual temperature (but not greater than ~~zero~~the melting point). Depending on the surface mass balance parametrisation, the latent heat release due to refreezing is transferred to the first ice layer.

A geothermal heat flux ϕ_0 is applied at the base of a 3 km thick bedrock layer with a Neumann boundary condition:

$$\phi_0 = -k_b \frac{\partial T}{\partial z}|_{bedrock} \tag{21}$$

with k_b the bedrock thermal conductivity.

Similarly to what is done for ice temperature, the heat equation is solved in the bedrock with Eq. 19 but with no advection nor heat production. From the temperature gradient in the bedrock (computed on four vertical levels) we compute a heat flux ϕ'_0 at the ice-bedrock interface. In case of ice dragging over the bedrock, an additional term due to friction, ϕ_f, is added to ϕ'_0:

$$\phi_f = |\mathbf{u}_b \, \tau_b| \tag{22}$$

The ice-bedrock interface heat flux is used differently for cold and temperate based points:

- For cold based points, the heat at the ice-bedrock interface is transferred to the ice via a Neumann boundary condition:

$$k_i \frac{\partial T}{\partial z}|_{ice} = -\phi'_0 - \phi_f \tag{23}$$

with the ice thermal conductivity k_i computed as:

$$k_i = 3.1014 \, 10^8 \, exp(-0.0057 \, (T + 273.15)) \tag{24}$$

- For temperate points, a Dirichlet boundary condition is applied as the temperature is kept at the pressure melting point. The excess heat in this case is used to compute basal melting:

$$b_{melt} = \frac{-\phi'_0 - \phi_f - k_i \frac{\partial T}{\partial z}|_{ice}}{L_f \rho_i} \quad \frac{-\phi'_0 - \phi_f - k_i \frac{\partial T}{\partial z}|_{ice}}{L_f \rho} \tag{25}$$

with L_f is the latent heat of fusion.

Basal melting for oceanic points is usually imposed. For specific applications we have different values for deep ocean and continental shelves, or a geographical distribution depending on the oceanic basin.

The viscosity for the velocity grid points is the horizontal average of the viscosity on the centred grid and not the viscosity computed from the horizontal average of the temperature. This is preferable for regions with mixed frozen and temperate basal conditions.

2.2 Additional features

2.2.1 Basal hydrology

Since the work of Peyaud (2006), GRISLI accounts for a simple diffusive basal hydrology scheme~~to calculate the water pressure.~~ . In the following we provide a complete description of the hydrology model because it has only been described in a French Phd dissertation (Peyaud, 2006) but currently lacks a description in an international scientific journal.

Using a Darcy law, the water produced by melting at the base of the ice sheet is routed outside glaciated areas following the highest gradient in the total water potential.

Such a gradient can be written as ~~:~~ in Shreve (1972):

$$\nabla\Phi = \rho_w g \nabla h_w + \rho_w g \nabla B + \rho_i g \nabla H \tag{26}$$

where ~~p_w is the water pressure~~h_w is the hydraulic head, B is the bedrock height and H the ice thickness.

In GRISLI, ~~water is supposed to flow within a thickness of 20 meters of till with a 50% porosity. Inside the till , assuming~~ we assume that the basal water flows within a sub-glacial till following a Darcy-type flow law~~, the water flux $\mathbf{Q}_w$ is proportional to the water potential gradient. For example in~~ :

$$\mathbf{Q_w} = -\frac{K D}{\rho_w g}\nabla\Phi \tag{27}$$

where $\mathbf{Q_w}$ is the water flux vector in x ~~direction:~~

$$Q_{wx} = -\frac{K\ D}{\rho_w g}\frac{\partial\Phi}{\partial x} = -\frac{K\ D}{\rho_w g}\frac{\partial}{\partial x}\left(\rho_w g \nabla B + \rho_i g \nabla H\right) - K\ D\frac{\partial h_w}{\partial x}$$

~~with h_w the hydraulic head~~ and y directions, K is the hydraulic conductivity of the till and D ~~the water depth in~~ is the water thickness within the till.

The till is assumed to be present everywhere below the ice sheet with a constant and homogeneous thickness ($h_{till} = 20\mathrm{m}$) and porosity ($\phi_{till} = 0.5$). The water thickness in the till, D, equals the hydraulic head, h_w, only for thicknesses lower than the effective thickness:

$$D = \min(h_w, \phi_{till} h_{till}) \tag{28}$$

The hydraulic conductivity of the till, K, is modulated by the effective pressure to take into account sediment dilatation:

$$K = \begin{cases} K_0 & \text{if } N > N_0 \\ K_0\ N_0/N & \text{if } N \leq N_0 \end{cases} \tag{29}$$

with K_0 the reference conductivity, N the effective pressure and N_0 a constant (~~$10^8 Pa$~~$10^8\mathrm{Pa}$). The conductivity K_0 is poorly constrained and strongly depends on the material.

~~The combination of~~ In GRISLI, we assume that the flow of water within the till can be described with a diffusivity equation for the hydraulic head:

$$\frac{\partial h_w}{\partial t} + \nabla.\mathbf{Q_w} = b_{melt} - I_{gr} \tag{30}$$

with I_{gr} being the infiltration rate in the bedrock (kept constant at 1 $\mathrm{mm\,yr^{-1}}$).

Using Eq. 26 and Eq. 27~~reduces to a diffusivity equation for the hydraulic head, h_w, which ultimately gives the water pressure, $p_w = \rho_w\, g\, h_w$.~~, this diffusivity equation can be written as:

$$\frac{\partial h_w}{\partial t} = b_{melt} - I_{gr} + \nabla.\left(KD\nabla\left(B + \frac{\rho}{\rho_w}H\right)\right) + \nabla.(KD\nabla h_w) \tag{31}$$

Similarly to what is done for the mass conservation equation a semi-implicit relaxation method is used to solve ~~the basal hydrology~~Eq. 31.

From the hydraulic head, h_w, we can compute the water pressure, $p_w = \rho_w\, g\, h_w$, and the effective pressure, $N = \rho\, g\, H - p_w$.

2.2.2 Isostasy

As in Ritz et al. (2001), GRISLI computes the bedrock response to ice load with an elastic lithosphere - relaxed asthenosphere (ELRA) model (Le Meur and Huybrechts, 1996). This simple model evaluates the bedrock deformation to a local unit mass, scaled to the whole ice sheet. The relaxation time of the asthenosphere is usually set to 3000 years and the deflection of the lithosphere is assumed to follow a zero-order Kelvin function. Such a simple model has been shown to perform well compared to more sophisticated glacio-isostatic models (Le Meur and Huybrechts, 1996).

2.2.3 Passive tracer

GRISLI includes a passive tracer model that allows for the computation of vertical ice stratigraphy, i.e. time and location of ice deposition for the vertical model grid points~~(Lhomme et al., 2005; Quiquet et al., 2013). For this, we~~ . The model is the one of Lhomme et al. (2005) re-implemented in GRISLI by Quiquet et al. (2013). We use a semi-Lagrangian scheme following Clark and Mix (2002) in order to avoid the numerical instabilities of Eulerian schemes and information dispersion of Lagrangian schemes (Rybak and Huybrechts, 2003). For each timestep, the back trajectories of each grid points are computed and tri-linearly interpolated onto the model grid. This allows for a continuous information within the ice sheet at a low computational cost. Time and location of ice deposition can be convoluted for example with isotopic composition of precipitation (e.g. $\delta^{18}O$) in order to construct synthetic ice cores comparable with actual ice cores (Lhomme et al., 2005).

2.3 Numerical features

The model uses finite differences computed on a staggered Arakawa C-grid in the horizontal plane ~~. The~~ (Fig. 2). In the vertical, the model defines σ-reduced coordinates, $\zeta = (S - z)/H$, for 21 evenly spaced vertical layers, with the z vertical axis pointing upward and ζ pointing downward (0 at the surface and 1 at the bottom). The coordinate triplet (i, j, k) (in x, y and ζ direction) is representative of the centre of the grid cell. The horizontal resolution depends on the application, i.e. the extension of the geographical domain and the duration of the simulated period. For century scale applications, the resolution varies from 5 km for Greenland to 15 km for Antarctica (Peano et al., 2017; Ritz et al., 2015). For multi-millenial applications the resolution ~~increases~~ reduces to 15 km for Greenland and 40 km for the whole Northern Hemisphere and Antarctica. ~~The~~

The mass balance equation is solved as an advection-only equation with an upwind scheme in space and a semi-implicit scheme in time (velocities at the previous time step are used). The numerical resolution is performed with a point-relaxation method with a variable time step. The value of this time step is chosen to ensure that the matrix becomes strongly diagonal dominant to achieve convergence of the point-relaxation method. The criteria is thus a threshold that is inversely proportional to the fastest velocity on the whole grid. Note that this smaller time step is solely used for the mass conservation equation (Eq. 2) and subsequent variables (e.g. surface slopes, SIA velocity) while the rest of the model uses a main time step, typically ranging from 0.5 to 5 years depending on the horizontal resolution. ~~Based on the maximum magnitude of the simulated velocity over the whole domain, the model computes a shorter time step for the mass conservation equation (Eq. 2)in order to avoid numerical instabilities~~

To solve it, the ice shelves/ice streams equation (Eq. 14) is linearised. The viscosity is computed using an iterative method starting from the viscosity calculated from strain rates from the previous time step. As this equation is the most expensive part of the model, the iteration mode is not always used depending on the type of experiment (for instance not crucial when the objective is to reach the steady state). In this case the viscosity of the previous time step is used. The linear system is solved with a direct method (Gaussian elimination, sgbsv in the Lapack library (www.netlib.org/lapack)).

The resolution of the elliptic system (Eq. 14) is the most expensive part of the model. This is further amplified by the ~~fact that, as in Ritz et al. (2001)~~way we prescribe boundary conditions. As in Ritz et al. (2001), the ice shelf region is artificially extended towards the edges of the geographical domain~~in order to get an ice front systematically parallel to either x or y~~. This artificial extension does not have any consequence on ice shelf velocity since added grid points (that we call "ghost"nodes) are prescribed with a negligible ice viscosity (~~1500 $Pa\,s$). In order to reduce~~ 1500 Pa s). The front is then parallel to either x or y (Ritz et al., 2001) and thus the boundary condition there is easy to implement (see also Fig. S1 in the supplement). The boundary condition at the real ice shelf front is implicitly done by solving (Eq. 14). However this method increases substantially the size of the linear system solved in (Eq. 14~~, we use~~). To go around, a simple reduction method ~~.~~ is implemented. (Eq. 14) can be written as ~~$A\,\mathbf{u} = B$ where $\mathbf{u}$~~ $\tilde{A}\,\tilde{\mathbf{u}} = \tilde{B}$ where $\tilde{\mathbf{u}}$ is a vector alternating u_x and u_y components for all the velocity grid points, ~~A~~ $\tilde{A}$ is a band matrix (very sparse) and ~~B~~ $\tilde{B}$ is a vector corresponding to the right hand terms in Eq. 14. ~~For~~ Every line of $\tilde{A}$ and $\tilde{B}$ are scaled so that the diagonal terms of $\tilde{A}$ are equal to 1. If, for a given velocity node~~(i.e. row i), if all the terms of column i in matrix A are small except A_{ii}~~, all the non diagonal terms of the column are very small compared to 1, this means that this node is actually not used by any other velocity node ~~. Row i can be therefore removedfrom the matrix. We use~~ and this line of the matrix can be removed. The threshold to neglect nodes is related to the value of the integrated viscosity of ~~artificial ice shelves (1500 $Pa\,s$) to define the threshold to neglect~~ "ghost" nodes . In practice, given its size, the matrix ~~A is not~~ $\tilde{A}$ is not actually fully constructed, only the non zero sub/sur diagonals are. An illustration of the matrix is shown in Fig. S2 in the supplement.

For the temperature equation (Eq. 19), we solved a 1D advection-diffusion equation for each model grid point. The resolution is performed with an upwind semi-implicit scheme (vertical velocity and heat production at the previous time step is used). The ice thermal conductivity is computed as the geometric mean of the two neighbouring conductivities (Patankar, 1980). Because the horizontal diffusion is neglected, the only horizontal terms concern horizontal advection and are computed with an upwind explicit scheme. The heat production is computed at the velocity (staggered) grid points and is then summed up to the temperature (centred) grid points.

The model has been recently partially parallelised with OpenMP (www.openmp.org), which considerably shortens the length of the simulations (gain of 40% for the Antarctic at 40 km on four threads of an Intel® Xeon® CPU@3.47 GHz).

3 Calibration for the Antartic ice sheet

3.1 Methods

In the following, we present a simple calibration methodology for the Antarctic ice sheet based on a large ensemble of model simulations. Given its degree of complexity, GRISLI is mostly designed for multi-millenial integrations. Due to long-term diffusive response to SMB and temperature changes, an accurate methodology to select unknown parameters of the model would be to run long transient simulations with a climate forcing as close as possible from past climate states, ideally with a synchronous coupling between the ice sheet and the atmosphere. However, climate models generally fail at reproducing the regional climate changes during the last glacial-interglacial cycle as recorded by proxy data (Braconnot et al., 2012). Furthermore, the phase III of the Paleoclimate Modelling Intercomparison Project (PMIP3) has highlighted the large disagreement between participating climate models in simulating the Last Glacial Maxium (LGM) in the vicinity of northern Hemisphere ice sheets (e.g. Harrison et al., 2014). Given these uncertainties amongst climate models and the large sensitivity of the ice sheet model to climate forcing fields (e.g. Charbit et al., 2007; Quiquet et al., 2012; Yan et al., 2013), it is difficult to calibrate the mechanical parameters independently from that of the SMB, in particular for northern Hemisphere ice sheets.

For these reasons, here we suggest a simple calibration methodology for the Antarctic ice sheet in which the model is run for 100 kyrs under a ~~constant~~ perpetual modern climate forcing in order to reach an ice sheet equilibrium. In the following, we use the 27 km-grid atmospheric outputs, namely annual mean temperature and SMB, from the regional climate model RACMO2~~2.3 (Noël et al., 2015)~~.3 (Van Wessem et al., 2014), averaged over the 1976-2016 time span. The basal melting rates under ice shelves are prescribed for the 18 sectors of the Antarctic ice sheet as defined in ISMIP-Antarctica ~~projet (~~project (Nowicki et al., 2016) and are shown in Fig. 3~~)~~. Their values are based on the sectoral average of sub-shelf melt rates that ensured stable ice shelves (minimal Eulerian ice thickness derivative) in the recent intercomparison exercise InitMIP-Antarctica (Nowicki et al., 2016), with slight modifications due to change in resolution. They are in line with observations-based estimates (Rignot et al., 2013). We do not apply any correction related to geometry changes to the climatic forcings during the calibration.

We choose to restrict this study to a coarse horizontal resolution, namely 40 km, as it allows for large ensembles of multi-millenial simulations. Whilst 6.7 hours on one thread of an Intel® Xeon® CPU@3.47 GHz (4 hours on four threads) are needed to perform 100 000 years of simulation over Antarctica on a 40-km grid (19 881 horizontal grid points), this time goes up significantly on a 16-km grid (145 161 points) for which we need 25 hours to perform 2000 years (17 hours on four threads). In addition, the 40 km resolution corresponds to the one used in the coupled version within the *i*LOVECLIM earth system model of intermediate complexity (Roche et al., 2014). Whilst with such a resolution we do not expect to have an accurate representation of the ice sheet fine scale structures such as ice streams, we expect to reproduce the large scale behaviour of ice flow.

From our experience with GRISLI, we identified four unknown parameters that have a crucial role for ice dynamics and that are independent from each other:

- The SIA flow enhancement factor ~~E_{SIA}~~ S_f of the Glen flow law (Eq. ~~11~~10). This coefficient is expected to have a large influence on shear-stress driven velocities.
- The basal drag coefficient C_f in Eq. 16. This coefficient is used to modulate the basal drag coefficient for temperate-based grid points where sliding occurs.
- The till conductivity K_0. This parameter changes the efficiency of basal water routing (Eq. 29 and Eq. 31) and thus, basal effective pressure N. As such, this parameter is also influencing the basal drag coefficient β for temperate-based regions (Eq. 16).
- An ice shelf basal melting rate coefficient ϕ_{shelf}. For a specific Antarctic ice shelf sector i:

$$BMB^i = \phi_{shelf} BMB_0^i \tag{32}$$

with BMB_0^i the sub-shelf basal melting rate reference values shown in Fig. 3. ~~Whilst the choice of BMB_0^i is based on the sectoral average of sub-shelf melt rates that ensured stable ice shelves in the recent intercomparison exercice InitMIP-Antarctica (Nowicki et al., 2016), with slight modifications due to change in resolution.~~

The parametric ensemble is designed with a Latin Hypercube Sampling (LHS) methodology. The LHS is used here because it has better space-filling quality than a standard Monte-Carlo sampling which might not explore sufficiently the tails of parameter distributions. This methodology has been used for calibration purposes in the ice sheet modelling community (e.g. Stone et al., 2010; Applegate et al., 2012). The size of the LHS consists ~~in 150~~ of 300 model realisations. We perform two times the ~~entire cube~~ 300 member ensemble with the flux at the grounding line of Schoof (2007) (hereafter AN40S) and Tsai et al. (2015) (hereafter AN40T) The range of explored parameters are listed in Tab. 2. We assume an uniform statistical distribution within this range.

The initial ice sheet geometry, bedrock and ice thickness, is taken from the Bedmap2 dataset (Fretwell et al., 2013) using

a spatial bi-linear interpolation to generate this data on the 40-km grid. The geothermal heat flux is from Shapiro and Ritzwoller (2004). Sensitivity to uncertainties in the forcing data are ~~discarded from~~ not explored in the ensemble as we aim at quantifying the model sensitivity to parameter choice even though we acknowledge for the fact that these could be the source of important model error (e.g. Stone et al., 2010; Pollard and DeConto, 2012).

3.2 Calibration results

~~Fig.~~Figure 4 presents the Antarctic ice sheet volumes at the end of the 100 kyr simulations for each ensemble members as a function of parameter values using the flux at the grounding line computed from Schoof (2007) (AN40S). We can see that there is a strong positive (respectively negative) correlation of ice volume with the basal drag coefficient (resp. enhancement factor). There is also a weak negative correlation for the sub-shelf basal melt coefficient~~. However, there is no~~ , and a weak positive correlation with the till conductivity. Since the global volume is an integrated metric that does not account for potential systematic compensation, ~~we computed~~ in Fig. 4 we also show the root mean square error (RMSE) in ice thickness for each ensemble members with respect to observations (Fretwell et al., 2013). ~~In Fig. 4, the red stars correspond to the ensemble members presenting~~ Amongst the 300 model realisations, 120 members present a RMSE lower than 350 m. ~~63 model realisations meet this criterion and~~ They are widespread across the range of parameter values. The lowest RMSE is ~~304~~294 m. The 12 best ensemble members are outlined in red in Fig. 4 and yield RMSE not higher than 304.

The general model response amongst the ensemble members is not fundamentally different when the flux at the grounding line is computed from Tsai et al. (2015) (Fig. 5). However, the grounding line position is much more unstable with a greater number of members showing lower ice sheet volume. Only ~~27~~ 62 model realisations present a RMSE lower than 350 m (lowest RMSE at ~~298 m~~ 295 m and 12 best not higher than 304), compared to ~~63~~ 120 within the AN40S ensemble members. This difference in term of grounding line stability for the two flux formulations has already been highlighted by Pattyn (2017). Since basal drag vanishes at the grounding line in the Tsai et al. (2015) formulation, its coefficient has a smaller impact than in Schoof (2007), amplifying the role of the ice flow enhancement factor. ~~For~~ As a consequence, for the AN40T ensemble, ~~this~~ the enhancement factor requires values between 1.5 and 3 in order to reach a good agreement with observed ice thickness, whilst values within 1.5 to ~~5~~ 4 are acceptable for AN40S.

In Fig. 6 (respectively Fig. 7) we show the ice thickness difference from the observations for the 12 ensemble members showing the lowest RMSE within the AN40S (resp. AN40T) model realisations. The differences are generally below 500 m even if persisting model biases are present across the ensemble members and model formulations. On the one hand, ice thickness in large parts of the East Antarctic ice sheet is systematically underestimated. On the other hand, the West Antarctic ice sheet shows more contrasted responses. Whilst for some ensemble members, the Ross embayment upstream region can be well represented (e.g. AN40S004 or AN40T065), the region feeding the Filchner-Ronne ice shelf show a quasi-systematic ice thickness underestimation. These model deficiencies can be attributed to our coarse model resolution, providing a poor representation of the complex bedrock structure in the Filchner-Ronne area. The model differences from the observations are very

similar to results from the PISM-PIK model shown in Martin et al. (2011) in term of amplitude but also in term of structure. They are also generally similar to Pollard and DeConto (2009). Consistent model biases amongst these models, which use different input data, suggest a common source of error related to the coarse model resolution (20 to 40 km) or uncertainties in the bedrock dataset, particularly large in East Antarctica (Fretwell et al., 2013).

Figure 8 (resp. Fig. ~~?? presents the~~ 9) presents the root mean square error with respect to observations of the ensemble members in the two-dimensional parametric space ~~. The ensemble members depicted in colours are the ones matching the selection criterion within~~ within AN40S ~~(red),~~ (resp. AN40T~~(blue) and for both of them (green)~~). The 12 best ensemble members are outlined in red. In most cases there is no clear relationship. However, there is a relationship emerging with a large basal drag coefficient being compensated by a large enhancement factor when using the Schoof (2007) ~~formulation (red and green stars~~(Fig. 8). When using the Tsai et al. (2015) formulation (~~blue and green stars~~Fig. 9), this relationship disappears as the enhancement factor is mostly driving the model response. A few model parameter combinations (30 out of 300) are able to provide a good representation of the present day Antarctic ice sheet, i.e. ~~low RMSE~~ RMSE lower than 350 m, independently from the grounding flux computation used (not shown).

Although our quality metric is based on the ice sheet thickness we show in Fig 10 and in Fig. 11 the capability of the model to reproduce observed ice sheet velocity (Mouginot et al., 2017) for the best ensemble members with the two formulations of the flux at the grounding line (parameter values shown in Tab. 3). The model reproduces the general distribution of the velocity although it underestimates ice flow for the very fast grid points (velocity larger than ~~100 $m\ yr^{-1}$~~ 100 $\mathrm{m\,yr^{-1}}$, generally ice shelves). The model has also difficulties to reproduce well-defined ice streams such as the Amery or Filchner ice shelves tributaries. These could be due to the coarse resolution used but also to the simple scheme used to estimate basal drag.

4 Antartic ice sheet changes for the last 400 kyrs

4.1 Methods

The main objective of this section is to show the ability of the model to reproduce large ice sheet geometry changes in response to Quaternary climate change. As a consequence of our limited knowledge of past climatic conditions in the Antarctic ice sheet region over glacial-interglacial cycles, we use here an idealised reconstruction of SMB, near surface air temperature and oceanic basal melting rates based on a limited number of proxy records. Our approach is ~~somehow~~ somewhat similar to previous works (e.g. Ritz et al., 2001; Huybrechts, 2002; Pollard and DeConto, 2009; Greve et al., 2011; Golledge et al., 2014).

The near-surface air temperature, used in the model as a surface boundary condition for the advection-diffusion temperature equation, is assumed to follow the EPICA-DOMEC deuterium record δD:

$$T_{palaeo} = T_0 + \left(1/\alpha^i\right) \delta D \tag{33}$$

with T_0 the annual mean near-surface air temperature from RACMO2.3 used for the present-day calibration. The isotopic slope for temperature, α^i, is set to ~~$0.18\,‰\,°C^{-1}$~~ $0.18\,‰\,°C^{-1}$ as in (Jouzel et al., 2007).

We also account for the additional temperature perturbation due to topography changes using a fixed and homogeneous lapse rate λ:

$$T^*_{palaeo} = T_{palaeo} + \lambda\,(S - S_0) \tag{34}$$

with $S - S_0$ the local topography change from Bedmap2. In the following λ is set to ~~$-8\,°C\,km^{-1}$~~ $-8\,°C\,km^{-1}$.

For a given near-surface air temperature change T^*_{palaeo} relative to present-day T_0, we modify the present-day SMB field, SMB_0:

$$SMB = SMB_0\ exp\left(-\gamma\left(T_0 - T^*_{palaeo}\right)\right) \tag{35}$$

with the precipitation ratio to temperature change γ set to ~~$0.07\,°C^{-1}$~~ $0.07\,°C^{-1}$. The use of an exponential form in Eq. 35 is motivated by the Clausius-Clapeyron saturation vapour pressure for an ideal gas. Such a simple expression implies that SMB is driven only by accumulation, an assumption justified by the very little surface ablation experienced by the Antarctic ice sheet under present-day climatic conditions. However, we may underestimate the surface melt for warmer past interglacial periods.

In order to account for changes in basal melting rates below ice shelves, there is the need to define a continuous proxy covering several glacial-interglacial cycles for past sub-surface oceanic conditions around Antarctica. To this end, and due to the lack of such a record in the Southern ocean, we used the temperature derived from a benthic foraminifer $\delta^{18}O$ record from the North Atlantic. This temperature signal is considered to depict the North Atlantic Deep Water (NADW) temperature (Waelbroeck et al., 2002). Here, we assume that changes in NADW temperature drive changes in the temperature of waters upwelled in the Southern Ocean. This upward flow separates into surface equatorward and poleward flows, and thus influences surface and sub-surface temperature around coastal Antarctica (e.g. Ferrari et al., 2014). The basal melting rate below a specific ice shelf sector i, BMB^i_{palaeo} for past periods is computed from its present-day value, BMB^i_0, corrected to account for past oceanic conditions:

$$BMB^i_{palaeo} = max\left(BMB^i_0\ (1 + \delta^{oc})\ ,\ 0.01\ m\ yr^{-1}\right) \tag{36}$$

using the palaeo-oceanic index δ^{oc} defined as:

$$\delta^{oc} = \alpha^{oc}\ \Delta T_{NA}/T_{NA0} \tag{37}$$

with T_{NA0} the pre-industrial temperature deduced from North Atlantic benthic foraminifera (Waelbroeck et al., 2002) and ΔT_{NA} the deviation from this temperature in the past. α^{oc} is a conversion coefficient, set to 1 in the following.

The atmospheric and oceanic indexes, $T_{palaeo} - T_0$ and δ^{oc}, used to drive the model for the last 400 kyr are presented in Fig. 12. In addition to these climatic perturbations we also use the eustatic sea level reconstruction of Waelbroeck et al. (2002) to account for sea level variations over glacial-interglacial cycles.

In the following, we discuss the model behaviour as the result to the 400 kyr forcing. We performed simulations using the 12 parameter combinations from Sec. 3 that yield the lowest RMSE for the two groups AN40S and AN40T, differing by the treatment of the flux at the grounding line. ~~The internal variables at the end of the 100 kyr under present-day constant climate forcing are used as initial conditions~~ We used the 100-kyr integration under perpetual modern climate in Sec. 3 as a spin-up for the transient simulations. We artificially expand the simulations for 10 kyr into the future with no climatic perturbation from the reference climate used in Sec. 3 in order to discuss the stability of the simulated present-day ice sheet state.

4.2 Transient simulation results

In Fig. 13 the simulated ice sheet volume is shown over the last 400 kyr. Across this time scale, a large glacial-interglacial volume variation is observed, in particular for the last two cycles where it reaches up to about 10 millions of ~~km^3~~ km^3. In our simulations, the Antarctic ice sheet volume increase at the last glacial maximum (LGM, 21 kaBP) relative to pre-industrial corresponds to about -10 to -20 m of global eustatic sea level drop depending on the simulations. These numbers mostly fall in the range of previous ice sheet model reconstructions (e.g. Huybrechts, 2002; Philippon et al., 2006; Pollard and DeConto, 2009), Antarctic contributions inferred as the difference from far-field and Northern Hemisphere near-field estimates (Peltier, 2004) or near-field estimates (Ivins and James, 2005; Argus et al., 2014; Whitehouse et al., 2012; Briggs et al., 2014). Our reconstructions are nonetheless at the higher hand of recent studies. This could be related to the fact that we do not account for different geologic bed types between today ice-free (with extensive amount of deformable till) and glaciated (mostly hard bed) continental shelf. To account for this, some authors have chosen a two-value basal drag for these different regions (e.g. Pollard and DeConto, 2012). Because of the large uncertainties related to the bed properties we have decided to ignore these differences, keeping in mind that this can bias our results towards thicker ice sheet when the ice expands over the continental shelf. In our simulations, the last interglacial (120 kaBP) ice volume does not present substantial changes relative to the present-day ice volume, as the Antarctic ice sheet is contributing to less than 6 centimetres to the global eustatic sea level rise in the simulations with the lowest RMSE at 0k. This is well below recent estimates, ranging from 3 to 7 m, inferred from the limited contribution of Greenland to the last interglacial highstand (Dutton et al., 2015). Our crude representation of the last interglacial climate in which no surface melt is possible may be the cause for such a discrepancy. In addition, our proxy-based basal melting rate does not allow for above than present basal melting rates during the last interglacial.

The uncertainty related to the choice of the internal parameters within our subset leads generally to up to ~~$3\ 10^6\ km^3$~~ $3\ 10^6\ km^3$ differences in our framework but do not change the model response to the forcings. In ~~turns~~turn, the choice of either Schoof (2007) (AN40S) or Tsai et al. (2015) (AN40T) to compute the flux at the grounding line leads to important differences amongst temporal model responses. AN40T systematically start to retreat before AN40S. It also produces a larger glacial to interglacial volume changes. This confirms the fact that the Tsai et al. (2015) formulation leads to more sensitive grounding line already highlighted in Sec. 3 and by other authors (Pattyn, 2017). The additional 10 kyr into the future with no climatic perturbation shows that the AN40S ensemble members do not produce an ice sheet at equilibrium at 0 ka BP. This means that, in our model,

the Schoof (2007) formulation produces unrealistically too slow post-LGM retreat which induces a model drift persisting till 10 kyr in the future. Conversely, the Tsai et al. (2015) formulation leads to more rapid retreat rates which provides a stabilisation of the ice sheet during the Holocene.

Simulated ice sheet surface elevations at selected snapshots for the two ensemble members with the lowest RMSE at 0 ka BP after the transient simulations are presented in Fig. 14. Ice sheet geometry during the last interglacial resembles the present-day one. This is particularly true for the eastern part whilst the West Antarctic ice sheet is only slightly thinner. At the last glacial maximum, the grounding line advances towards the edge of the continental shelf, in agreement with geological reconstructions (Bentley et al., 2014). The choice of the flux at the grounding line formulation has an impact on the maximum ice sheet extent, with a less extended ice sheet using the Schoof (2007) formulation. As for the last interglacial, the eastern part of the ice sheet presents only small variations in surface elevation compared to the present-day geometry. There is no decrease in surface elevation at the last glacial maximum due to reduction in precipitation at this time since the larger extent and the colder climate tend to reduce the ice flow. The largest topography changes are occurring in the Weddel and Ross sea. The West Antarctic ice sheet is thus particularly dynamic during glacial-interglacial cycles.

The RMSE computed at 0 ka BP for the 24 members used for the transient simulations ranges from 372 to 467 m within AN40S and 326 to 376 m within AN40T. These numbers are only slightly greater than the ones obtained using a constant forcing (Sec. 3). The differences in ice sheet thickness between the transient simulations at 0 ka BP and the observations for the two ensemble members with the lowest RMSE (AN40S097 and AN40T059) are shown in Fig. 15. The pattern is similar to the one obtained during the calibration step (Sec. 3) with some notable differences. On the one hand, the East Antarctic ice sheet thickness underestimation is partly corrected when performing a transient simulation. This could be the result of a better representation of the temperature vertical profile in this case. On the other hand, whilst in other regions the model biases remain generally the same between an equilibrium and a transient simulation, important model biases appear at the margins of the ice sheet when using the transient simulations. This is particularly visible when using Schoof (2007) for which the retreat rate during the deglaciation is underestimated. Part of the misrepresentation of present-day margins could also be due to the over-simplified climatic perturbation used for the transient simulations.

5 Discussion and outlook

We have presented results from the updated version of the GRISLI model. Whilst the model is able to reproduce present-day Greenland (Le clec'h et al., 2017) and Antarctic (Ritz et al., 2015) ice sheets when using an inverse method to estimate the basal drag, our simulations with an interactive basal drag coefficients computed from the effective pressure show some important disagreements relative to observations. In particular there are some persisting model biases in ice thickness~~: underestimation (resp. overestimation) of southern (resp. northern) part of East Antarctic and underestimation (resp. overestimation) of~~ . In East Antarctica, the ice thickness is underestimated towards the pole and the Transantarctic mountains while it is overestimated

towards the margins, from Queen Maud land to Wilkes land. In West Antarctica, there is an underestimation of ice thickness in the Ronnie-Filchner ~~(resp. Ross) basins~~basin and an overestimation in the Ross basin. These model biases are also present in models of similar complexity when using an interactive basal drag computation (Pollard and DeConto, 2009; Martin et al., 2011). This data-model mismatch is mostly due to a poor representation of the bedrock-ice interface. In particular, the coarse resolution does not allow for the consideration of fine scale troughs and pinning points. The persisting model biases can be also the consequence of our simplified basal drag computation that does not take into account bedrock physical properties (e.g. sediments).

We used a basal drag coefficient computed from an internal model parameter, namely the basal effective pressure. For long-term multi-millenial integrations, this is preferred to basal drag coefficient deduced from inversion using present-day geometry since it is fully consistent with the model physics and, in principle, remains valid for large ice sheet geometry change. However, by design, the fit with observations is systematically poorer compared to ~~results from inversion~~model results that make use of an inverse basal drag coefficient. A step forward would be to use the basal drag computed from inversion in order to ~~infer~~ deduce a formulation based solely on internal parameters. Amongst these parameters, along with the basal effective pressure, the large scale bedrock curvature and/or sub-grid roughness could be used, similarly to Briggs et al. (2013). ~~To progress further on this topic, the implementation of a new basal hydrology model relying on explicit routing scheme (e.g. Kavanagh and Tarasov, 2017) would allow to avoid relaxed numerical solutions based on effective pressure. This could introduce fast basal water changes that are currently ignored and, ultimately, could yield ice streams abrupt speed-up or slow-down~~However, some key basal features, such as the geologic bed type and the deformable till distribution, remain today largely unknown below present-day ice sheets and will contribute to large uncertainties in the basal drag formulation.

Although widely used for ice sheet model spin-up or calibration, long-term integrations under present-day forcing induce ~~misrepresentation of~~ a warm bias in the vertical temperature profile because they discard the diffusion of glacial-interglacial changes in surface temperature. Calibrated parameters obtained with such a methodology tend to compensate for the under-estimated viscosity and are in theory not suitable for palaeo-reconstructions. Whilst a parameter calibration based on glacial-interglacial simulations is ideally preferred, the determination of a realistic climate forcing is a considerable challenge given the many degrees of freedom. Here, we presented a very simplified climate reconstructions for the last 400 kyr based on a minimal parameter set (proxy for atmospheric temperatures and oceanic conditions) in order to illustrate the model possible behaviour for long-term integrations. Further work will consist in the determination of more realistic climate reconstruction using general circulation model snapshots. We also aim at expanding the work of Roche et al. (2014) and couple the Antarctic geometry of GRISLI version 2.0 with the *i*LOVECLIM model.

The implementation of an explicit flux computation at the grounding line following Schoof (2007) and Tsai et al. (2015) lead to a more ~~unstable position of the grounding line~~ dynamic grounding line position compared to previous version of the model. As such, GRISLI version 2.0 is now more sensitive to ~~change in sea level~~ both sub-shelf melt rate changes and also

sea level variations. However, the current version of the model only considers an eustatic sea level perturbation with a regional bedrock adjustment. The explicit computation of local relative sea level could potentially have an important impact on grounding line migration for glacial-interglacial cycles (e.g. Gomez et al., 2013).

Calving In the current version of the model, some important processes are still largely simplified. In particular, further developments will consist in the implementation of a new basal hydrology model relying on explicit routing scheme (e.g. Kavanagh and Tara allow to avoid relaxed numerical solutions based on effective pressure. This could introduce fast basal water changes that are currently ignored and, ultimately, could yield ice streams abrupt speed-up or slow-down. Also, calving processes are suspected to be a major driver for ice sheet evolution due to the importance of buttressing on inland ice dynamics (e.g. Pollard et al., 2015). GRISLI v2 version 2.0 includes a very simplified calving representation that might prevent to assess the role of this process for multi-millenial ice dynamics. The inclusion of a physically based calving scheme (e.g. Christmann et al., 2016) would be a significant model improvement for future model revisions.

6 Conclusions

We have presented the GRISLI (version 2.0) model along with the significant improvements from the previous version of Ritz et al. (2001). Such improvements include an explicit flux computation at the grounding line, an interactive basal hydrology module and a semi-lagrangian tracking particle scheme. Thanks to its low computational cost, the model is suitable for long-term multi-millenial integrations. We performed a large ensemble of simulations of the Antarctic ice sheet forced by present-day climate conditions to calibrate the crucial unknown parameters. We have shown that the model is able to reproduce reasonably well the present-day geometry although the grounding line position in the model is much more unstable when we use Tsai et al. (2015) formulation of the flux at the grounding line instead of Schoof (2007). The model mismatch with respect to observed ice thickness shows some systematic biases (e.g. the East Antarctic ice sheet is too thick in the vicinity of the Transantarctic mountains and too thin elsewhere), that are similar to models of comparable complexity. We used the best ensemble members to simulate the Antarctic evolution throughout the last 400 kyr using an idealised climatic perturbation of present-day conditions. With this simple framework we reproduced the expected ice sheet geometry changes over glacial-interglacial cycles. A significant volume increase is simulated during glacial periods with a grounding line advance towards the edge of the continental shelf. The retreat during terminations is gradual when using our forcing scenario and is able to produce a final present-day ice volume and extent similar to observations. The Tsai et al. (2015) formulation produces a faster ice sheet retreat and yields an ice sheet near equilibrium during the Holocene contrary to Schoof (2007) for which the model is still drifting at +10 kyr into the future. This suggests that, in our model and under the climate forcing scenario we use, the Tsai et al. (2015) formulation produces a more realistic grounding line retreat rate. The validation of the model for the Antarctic ice sheet changes through glacial-interglacial cycles give confidence in ice dynamics in the model and its applicability to northern Hemisphere ice sheets.

7 Code availability

The developments on the GRISLI source code are hosted at https://forge.ipsl.jussieu.fr/grisli, but are not publicly available due to copyright restrictions. Access can be granted on demand by request to ~~Catherine Ritz (catherine.ritz@univ-grenoble-alpes.fr),~~ Christophe Dumas (christophe.dumas@lsce.ipsl.fr)~~and~~ , Aurélien Quiquet (aurelien.quiquet@lsce.ipsl.fr) or Catherine Ritz (catherine.ritz@univ-grenoble-alpes.fr) to those who conduct research in collaboration with the GRISLI users group. For this work we used the model at revision 188.

Acknowledgements. We thank Michiel van den Broeke (IMAU, Utrecht University) for providing the RACMO2~~2.3~~ 3 model outputs. We also warmly thank Claire Waelbroeck for fruitful discussions on the construction of the index for sub-shelf melting rates. This is a contribution to ERC project ACCLIMATE; the research leading to these results has received funding from the European Research Council under the European Union's Seventh Framework Programme (FP7/2007-2013)/ERC grant agreement 339108.

References

Abe-Ouchi, A., Saito, F., Kawamura, K., Raymo, M. E., Okuno, J., Takahashi, K., and Blatter, H.: Insolation-driven 100,000-year glacial cycles and hysteresis of ice-sheet volume, Nature, 500, 190–193, doi:10.1038/nature12374, 2013.

Alvarez-Solas, J., Charbit, S., Ritz, C., Paillard, D., Ramstein, G., and Dumas, C.: Links between ocean temperature and iceberg discharge during Heinrich events, Nature Geosci, 3, 122–126, doi:10.1038/ngeo752, 2010.

Alvarez-Solas, J., Robinson, A., Montoya, M., and Ritz, C.: Iceberg discharges of the last glacial period driven by oceanic circulation changes, Proceedings of the National Academy of Sciences, 110, 16 350–16 354, doi:10.1073/pnas.1306622110, 2013.

Applegate, P. J., Kirchner, N., Stone, E. J., Keller, K., and Greve, R.: An assessment of key model parametric uncertainties in projections of Greenland Ice Sheet behavior, The Cryosphere, 6, 589–606, doi:10.5194/tc-6-589-2012, 2012.

Argus, D. F., Peltier, W. R., Drummond, R., and Moore, A. W.: The Antarctica component of postglacial rebound model ICE-6G_C (VM5a) based on GPS positioning, exposure age dating of ice thicknesses, and relative sea level histories, Geophysical Journal International, 198, 537–563, doi:10.1093/gji/ggu140, 2014.

Benn, D. I., Le Hir, G., Bao, H., Donnadieu, Y., Dumas, C., Fleming, E. J., Hambrey, M. J., McMillan, E. A., Petronis, M. S., Ramstein, G., Stevenson, C. T. E., Wynn, P. M., and Fairchild, I. J.: Orbitally forced ice sheet fluctuations during the Marinoan Snowball Earth glaciation, Nature Geoscience, 8, 704–707, doi:10.1038/ngeo2502, 2015.

Bentley, M. J., Ó Cofaigh, C., Anderson, J. B., Conway, H., Davies, B., Graham, A. G. C., Hillenbrand, C.-D., Hodgson, D. A., Jamieson, S. S. R., Larter, R. D., Mackintosh, A., Smith, J. A., Verleyen, E., Ackert, R. P., Bart, P. J., Berg, S., Brunstein, D., Canals, M., Colhoun, E. A., Crosta, X., Dickens, W. A., Domack, E., Dowdeswell, J. A., Dunbar, R., Ehrmann, W., Evans, J., Favier, V., Fink, D., Fogwill, C. J., Glasser, N. F., Gohl, K., Golledge, N. R., Goodwin, I., Gore, D. B., Greenwood, S. L., Hall, B. L., Hall, K., Hedding, D. W., Hein, A. S., Hocking, E. P., Jakobsson, M., Johnson, J. S., Jomelli, V., Jones, R. S., Klages, J. P., Kristoffersen, Y., Kuhn, G., Leventer, A., Licht, K., Lilly, K., Lindow, J., Livingstone, S. J., Massé, G., McGlone, M. S., McKay, R. M., Melles, M., Miura, H., Mulvaney, R., Nel, W., Nitsche, F. O., O'Brien, P. E., Post, A. L., Roberts, S. J., Saunders, K. M., Selkirk, P. M., Simms, A. R., Spiegel, C., Stolldorf, T. D., Sugden, D. E., van der Putten, N., van Ommen, T., Verfaillie, D., Vyverman, W., Wagner, B., White, D. A., Witus, A. E., and Zwartz, D.: A community-based geological reconstruction of Antarctic Ice Sheet deglaciation since the Last Glacial Maximum, Quaternary Science Reviews, 100, 1–9, doi:10.1016/j.quascirev.2014.06.025, 2014.

Bindschadler, R.: The Importance of Pressurized Subglacial Water in Separation and Sliding at the Glacier Bed, Journal of Glaciology, 29, 3–19, doi:10.3189/S0022143000005104, 1983.

Braconnot, P., Harrison, S. P., Kageyama, M., Bartlein, P. J., Masson-Delmotte, V., Abe-Ouchi, A., Otto-Bliesner, B., and Zhao, Y.: Evaluation of climate models using palaeoclimatic data, Nature Climate Change, 2, 417–424, doi:10.1038/nclimate1456, 2012.

Briggs, R., Pollard, D., and Tarasov, L.: A glacial systems model configured for large ensemble analysis of Antarctic deglaciation, The Cryosphere, 7, 1949–1970, doi:10.5194/tc-7-1949-2013, 2013.

Briggs, R. D., Pollard, D., and Tarasov, L.: A data-constrained large ensemble analysis of Antarctic evolution since the Eemian, Quaternary Science Reviews, 103, 91–115, doi:10.1016/j.quascirev.2014.09.003, 2014.

Bueler, E. and Brown, J.: Shallow shelf approximation as a "sliding law" in a thermomechanically coupled ice sheet model, Journal of Geophysical Research: Earth Surface, 114, F03 008, doi:10.1029/2008JF001179, 2009.

Calov, R., Greve, R., Abe-Ouchi, A., Bueler, E., Huybrechts, P., Johnson, J. V., Pattyn, F., Pollard, D., Ritz, C., Saito, F., and Tarasov, L.: Results from the Ice-Sheet Model Intercomparison Project–Heinrich Event Intercomparison (ISMIP HEINO), Journal of Glaciology, 56, 371–383, doi:10.3189/002214310792447789, 2010.

Charbit, S., Ritz, C., Philippon, G., Peyaud, V., and Kageyama, M.: Numerical reconstructions of the Northern Hemisphere ice sheets through the last glacial-interglacial cycle, Climate of the Past, 3, 15–37, doi:10.5194/cp-3-15-2007, 2007.

Christmann, J., Plate, C., Müller, R., and Humbert, A.: Viscous and viscoelastic stress states at the calving front of Antarctic ice shelves, Annals of Glaciology, 57, 10–18, doi:10.1017/aog.2016.18, 2016.

Clark, P. U. and Mix, A. C.: Ice sheets and sea level of the Last Glacial Maximum, Quaternary Science Reviews, 21, 1–7, doi:10.1016/S0277-3791(01)00118-4, 2002.

Colleoni, F., Kirchner, N., Niessen, F., Quiquet, A., and Liakka, J.: An East Siberian ice shelf during the Late Pleistocene glaciations: Numerical reconstructions, Quaternary Science Reviews, 147, 148–163, doi:10.1016/j.quascirev.2015.12.023, 2016.

Deschamps, P., Durand, N., Bard, E., Hamelin, B., Camoin, G., Thomas, A. L., Henderson, G. M., Okuno, J., and Yokoyama, Y.: Ice-sheet collapse and sea-level rise at the Bølling warming 14,600 years ago, Nature, 483, 559, doi:10.1038/nature10902, 2012.

Donnadieu, Y., Dromart, G., Goddéris, Y., Pucéat, E., Brigaud, B., Dera, G., Dumas, C., and Olivier, N.: A mechanism for brief glacial episodes in the Mesozoic greenhouse, Paleoceanography, 26, PA3212, doi:10.1029/2010PA002100, 2011.

Dumas, C.: Modélisation de l'évolution de l'Antarctique depuis le dernier cycle glaciaire-interglaciaire jusqu'au futur : importance relative des différents processus physiques et rôle des données d'entrée, Ph.D. thesis, Université Joseph-Fourier - Grenoble I, 2002.

Durand, G., Gagliardini, O., de Fleurian, B., Zwinger, T., and Le Meur, E.: Marine ice sheet dynamics: Hysteresis and neutral equilibrium, Journal of Geophysical Research: Earth Surface, 114, F03 009, doi:10.1029/2008JF001170, 2009.

Dutton, A., Carlson, A. E., Long, A. J., Milne, G. A., Clark, P. U., DeConto, R., Horton, B. P., Rahmstorf, S., and Raymo, M. E.: Sea-level rise due to polar ice-sheet mass loss during past warm periods, Science, 349, aaa4019, doi:10.1126/science.aaa4019, 2015.

Duval, P. and Lliboutry, L.: Superplasticity owing to grain growth in polar ices, Journal of Glaciology, 31, 60–62, 1985.

Edwards, T. L., Fettweis, X., Gagliardini, O., Gillet-Chaulet, F., Goelzer, H., Gregory, J. M., Hoffman, M., Huybrechts, P., Payne, A. J., Perego, M., Price, S., Quiquet, A., and Ritz, C.: Effect of uncertainty in surface mass balance–elevation feedback on projections of the future sea level contribution of the Greenland ice sheet, The Cryosphere, 8, 195–208, doi:10.5194/tc-8-195-2014, 2014.

Fairbanks, R. G.: A 17,000-year glacio-eustatic sea level record: influence of glacial melting rates on the Younger Dryas event and deep-ocean circulation, Nature, 342, 637, doi:10.1038/342637a0, 1989.

Favier, L., Durand, G., Cornford, S. L., Gudmundsson, G. H., Gagliardini, O., Gillet-Chaulet, F., Zwinger, T., Payne, A. J., and Brocq, A. M. L.: Retreat of Pine Island Glacier controlled by marine ice-sheet instability, Nature Climate Change, 4, 117, doi:10.1038/nclimate2094, 2014.

Ferrari, R., Jansen, M. F., Adkins, J. F., Burke, A., Stewart, A. L., and Thompson, A. F.: Antarctic sea ice control on ocean circulation in present and glacial climates, Proceedings of the National Academy of Sciences, 111, 8753–8758, doi:10.1073/pnas.1323922111, 2014.

Fretwell, P., Pritchard, H. D., Vaughan, D. G., Bamber, J. L., Barrand, N. E., Bell, R., Bianchi, C., Bingham, R. G., Blankenship, D. D., Casassa, G., Catania, G., Callens, D., Conway, H., Cook, A. J., Corr, H. F. J., Damaske, D., Damm, V., Ferraccioli, F., Forsberg, R., Fujita, S., Gim, Y., Gogineni, P., Griggs, J. A., Hindmarsh, R. C. A., Holmlund, P., Holt, J. W., Jacobel, R. W., Jenkins, A., Jokat, W., Jordan, T., King, E. C., Kohler, J., Krabill, W., Riger-Kusk, M., Langley, K. A., Leitchenkov, G., Leuschen, C., Luyendyk, B. P., Matsuoka, K., Mouginot, J., Nitsche, F. O., Nogi, Y., Nost, O. A., Popov, S. V., Rignot, E., Rippin, D. M., Rivera, A., Roberts, J., Ross, N., Siegert, M. J., Smith, A. M., Steinhage, D., Studinger, M., Sun, B., Tinto, B. K., Welch, B. C., Wilson, D., Young, D. A., Xiangbin, C., and Zirizzotti,

A.: Bedmap2: improved ice bed, surface and thickness datasets for Antarctica, The Cryosphere, 7, 375–393, doi:10.5194/tc-7-375-2013, 2013.

Fürst, J.: Dynamic response of the Greenland ice sheet to future climatic warming, Ph.D. thesis, Vrije Universiteit Brussel, Brussel, 2013.

Gillet-Chaulet, F., Gagliardini, O., Seddik, H., Nodet, M., Durand, G., Ritz, C., Zwinger, T., Greve, R., and Vaughan, D. G.: Greenland ice sheet contribution to sea-level rise from a new-generation ice-sheet model, The Cryosphere, 6, 1561–1576, doi:10.5194/tc-6-1561-2012, 2012.

Goelzer, H., Nowicki, S., Edwards, T., Beckley, M., Abe-Ouchi, A., Aschwanden, A., Calov, R., Gagliardini, O., Gillet-Chaulet, F., Golledge, N. R., Gregory, J., Greve, R., Humbert, A., Huybrechts, P., Kennedy, J. H., Larour, E., Lipscomb, W. H., Le clec´h, S., Lee, V., Morlighem, M., Pattyn, F., Payne, A. J., Rodehacke, C., Rückamp, M., Saito, F., Schlegel, N., Seroussi, H., Shepherd, A., Sun, S., van de Wal, R., and Ziemen, F. A.: Design and results of the ice sheet model initialisation experiments initMIP-Greenland: an ISMIP6 intercomparison, The Cryosphere Discuss., 2017, 1–42, doi:10.5194/tc-2017-129, 2017.

Golledge, N. R., Menviel, L., Carter, L., Fogwill, C. J., England, M. H., Cortese, G., and Levy, R. H.: Antarctic contribution to meltwater pulse 1A from reduced Southern Ocean overturning, Nature Communications, 5, 5107, doi:10.1038/ncomms6107, 2014.

Gomez, N., Pollard, D., and Mitrovica, J. X.: A 3-D coupled ice sheet – sea level model applied to Antarctica through the last 40 ky, Earth and Planetary Science Letters, 384, 88–99, doi:10.1016/j.epsl.2013.09.042, 2013.

Gregoire, L. J., Payne, A. J., and Valdes, P. J.: Deglacial rapid sea level rises caused by ice-sheet saddle collapses, Nature, 487, 219, doi:10.1038/nature11257, 2012.

Greve, R., Saito, F., and Abe-Ouchi, A.: Initial results of the SeaRISE numerical experiments with the models SICOPOLIS and IcIES for the Greenland ice sheet, Annals of Glaciology, 52, 23–30, doi:10.3189/172756411797252068, 2011.

Hall, D. K., Comiso, J. C., DiGirolamo, N. E., Shuman, C. A., Box, J. E., and Koenig, L. S.: Variability in the surface temperature and melt extent of the Greenland ice sheet from MODIS, Geophysical Research Letters, 40, 2114–2120, doi:10.1002/grl.50240, 2013.

Hanebuth, T., Stattegger, K., and Grootes, P. M.: Rapid Flooding of the Sunda Shelf: A Late-Glacial Sea-Level Record, Science, 288, 1033–1035, doi:10.1126/science.288.5468.1033, 2000.

Harrison, S. P., Bartlein, P. J., Brewer, S., Prentice, I. C., Boyd, M., Hessler, I., Holmgren, K., Izumi, K., and Willis, K.: Climate model benchmarking with glacial and mid-Holocene climates, Climate Dynamics, 43, 671–688, doi:10.1007/s00382-013-1922-6, 2014.

Hindmarsh, R. C. A.: A numerical comparison of approximations to the Stokes equations used in ice sheet and glacier modeling, Journal of Geophysical Research: Earth Surface, 109, F01 012, doi:10.1029/2003JF000065, 2004.

Hutter, K.: A mathematical model of polythermal glaciers and ice sheets, Geophysical & Astrophysical Fluid Dynamics, 21, 201–224, doi:10.1080/03091928208209013, 1982.

Hutter, K.: Theoretical glaciology: material science of ice and the mechanics of glaciers and ice sheets, Springer, 1983.

Huybrechts, P.: Sea-level changes at the LGM from ice-dynamic reconstructions of the Greenland and Antarctic ice sheets during the glacial cycles, Quaternary Science Reviews, 21, 203–231, doi:10.1016/S0277-3791(01)00082-8, 2002.

Ivins, E. R. and James, T. S.: Antarctic glacial isostatic adjustment: a new assessment, Antarctic Science, 17, 541–553, doi:10.1017/S0954102005002968, 2005.

Jouzel, J., Masson-Delmotte, V., Cattani, O., Dreyfus, G., Falourd, S., Hoffmann, G., Minster, B., Nouet, J., Barnola, J. M., Chappellaz, J., Fischer, H., Gallet, J. C., Johnsen, S., Leuenberger, M., Loulergue, L., Luethi, D., Oerter, H., Parrenin, F., Raisbeck, G., Raynaud, D., Schilt, A., Schwander, J., Selmo, E., Souchez, R., Spahni, R., Stauffer, B., Steffensen, J. P., Stenni, B., Stocker, T. F., Tison, J. L.,

Werner, M., and Wolff, E. W.: Orbital and Millennial Antarctic Climate Variability over the Past 800,000 Years, Science, 317, 793–796, doi:10.1126/science.1141038, 2007.

Kavanagh, M. and Tarasov, L.: BrAHMs V1.0: A fast, physically-based subglacial hydrology model for continental-scale application, Geosci. Model Dev. Discuss., 2017, 1–20, doi:10.5194/gmd-2017-275, 2017.

Koenig, S. J., Dolan, A. M., de Boer, B., Stone, E. J., Hill, D. J., DeConto, R. M., Abe-Ouchi, A., Lunt, D. J., Pollard, D., Quiquet, A., Saito, F., Savage, J., and van de Wal, R.: Ice sheet model dependency of the simulated Greenland Ice Sheet in the mid-Pliocene, Climate of the Past, 11, 369–381, doi:10.5194/cp-11-369-2015, 2015.

Ladant, J.-B., Donnadieu, Y., Lefebvre, V., and Dumas, C.: The respective role of atmospheric carbon dioxide and orbital parameters on ice sheet evolution at the Eocene-Oligocene transition, Paleoceanography, 29, 2013PA002 593, doi:10.1002/2013PA002593, 2014.

Larour, E., Seroussi, H., Morlighem, M., and Rignot, E.: Continental scale, high order, high spatial resolution, ice sheet modeling using the Ice Sheet System Model (ISSM), Journal of Geophysical Research: Earth Surface, 117, F01 022, doi:10.1029/2011JF002140, 2012.

Le clec'h, S., Fettweis, X., Quiquet, A., Dumas, C., Kageyama, M., Charbit, S., Wyard, C., and Ritz, C.: Assessment of the Greenland ice sheet – atmosphere feedbacks for the next century with a regional atmospheric model fully coupled to an ice sheet model, The Cryosphere Discuss., 2017, 1–31, doi:10.5194/tc-2017-230, 2017.

Le clec'h, S., Quiquet, A., Charbit, S., Dumas, C., Kageyama, M., and Ritz, C.: A rapidly converging spin-up method for the present-day Greenland ice sheet using the GRISLI ice-sheet model, Geosci. Model Dev. Discuss., 2018, 1–21, doi:10.5194/gmd-2017-322, 2018.

Le Gac, H.: Contribution à la détermination des lois de comportement de la glace polycristalline (anélasticité et plasticité), Ph.D. thesis, Université Joseph-Fourier - Grenoble I, 1980.

Le Meur, E. and Huybrechts, P.: A comparison of different ways of dealing with isostasy: examples from modeling the Antarctic ice sheet during the last glacial cycle, Annals of Glaciology, 23, 309–317, 1996.

Lhomme, N., Clarke, G. K., and Marshall, S. J.: Tracer transport in the Greenland Ice Sheet: constraints on ice cores and glacial history, Quaternary Science Reviews, 24, 173–194, doi:10.1016/j.quascirev.2004.08.020, 2005.

Lipenkov, V. Y., Salamatin, A. N., and Duval, P.: Bubbly-ice densification in ice sheets: II. Applications, Journal of Glaciology, 43, 397–407, doi:10.3189/S0022143000034973, 1997.

Ma, Y., Gagliardini, O., Ritz, C., Gillet-Chaulet, F., Durand, G., and Montagnat, M.: Enhancement factors for grounded ice and ice shelves inferred from an anisotropic ice-flow model, Journal of Glaciology, 56, 805–812, doi:10.3189/002214310794457209, 2010.

MacAyeal, D. R.: Large-Scale Ice Flow Over a Viscous Basal Sediment: Theory and Application to Ice Stream B, Antarctica, Journal of Geophysical Research, 94, pp. 4071–4087, doi:198910.1029/JB094iB04p04071, 1989.

Martin, M. A., Winkelmann, R., Haseloff, M., Albrecht, T., Bueler, E., Khroulev, C., and Levermann, A.: The Potsdam Parallel Ice Sheet Model (PISM-PIK) – Part 2: Dynamic equilibrium simulation of the Antarctic ice sheet, The Cryosphere, 5, 727–740, doi:10.5194/tc-5-727-2011, 2011.

Mouginot, J., Rignot, E., Scheuchl, B., Fenty, I., Khazendar, A., Morlighem, M., Buzzi, A., and Paden, J.: Fast retreat of Zachariæ Isstrøm, northeast Greenland, Science, 350, 1357–1361, doi:10.1126/science.aac7111, 2015.

Mouginot, J., Rignot, E., Scheuchl, B., and Millan, R.: Comprehensive Annual Ice Sheet Velocity Mapping Using Landsat-8, Sentinel-1, and RADARSAT-2 Data, Remote Sensing, 9, 364, doi:10.3390/rs9040364, 2017.

Nowicki, S. M. J., Payne, A., Larour, E., Seroussi, H., Goelzer, H., Lipscomb, W., Gregory, J., Abe-Ouchi, A., and Shepherd, A.: Ice Sheet Model Intercomparison Project (ISMIP6) contribution to CMIP6, Geosci. Model Dev., 9, 4521–4545, doi:10.5194/gmd-9-4521-2016, 2016.

Noël, B., van de Berg, W. J., van Meijgaard, E., Kuipers Munneke, P., van de Wal, R. S. W., and van den Broeke, M. R.: Evaluation of the updated regional climate model RACMO2.3: summer snowfall impact on the Greenland Ice Sheet, The Cryosphere, 9, 1831–1844, doi:10.5194/tc-9-1831-2015, 2015.

Paolo, F. S., Fricker, H. A., and Padman, L.: Volume loss from Antarctic ice shelves is accelerating, Science, 348, 327–331, doi:10.1126/science.aaa0940, 2015.

Patankar, S. V.: Numerical heat transfer and fluid flow, Taylor & Francis, Washington, DC,, 1980.

Pattyn, F.: Sea-level response to melting of Antarctic ice shelves on multi-centennial timescales with the fast Elementary Thermomechanical Ice Sheet model (f.ETISh v1.0), The Cryosphere, 11, 1851–1878, doi:10.5194/tc-11-1851-2017, 2017.

Peano, D., Colleoni, F., Quiquet, A., and Masina, S.: Ice flux evolution in fast flowing areas of the Greenland ice sheet over the 20th and 21st centuries, Journal of Glaciology, 63, 499–513, doi:10.1017/jog.2017.12, 2017.

Peltier, W. R.: Global glacial isostasy and the surface of the Ice-Age Earth: The ICE-5G (VM2) Model and GRACE, Annual Review of Earth and Planetary Sciences, 32, 111–149, doi:10.1146/annurev.earth.32.082503.144359, 2004.

Pettit, E. C. and Waddington, E. D.: Ice flow at low deviatoric stress, Journal of Glaciology, 49, 359–369, doi:10.3189/172756503781830584, 2003.

Peyaud, V.: Rôle de la dynamique des calottes glaciaires dans les grands changements climatiques des périodes glaciaires-interglaciaires., Ph.D. thesis, Université Joseph-Fourier - Grenoble I, 2006.

Peyaud, V., Ritz, C., and Krinner, G.: Modelling the Early Weichselian Eurasian Ice Sheets: role of ice shelves and influence of ice-dammed lakes, Climate of the Past, 3, 375–386, doi:10.5194/cp-3-375-2007, 2007.

Philippon, G., Ramstein, G., Charbit, S., Kageyama, M., Ritz, C., and Dumas, C.: Evolution of the Antarctic ice sheet throughout the last deglaciation: A study with a new coupled climate–north and south hemisphere ice sheet model, Earth and Planetary Science Letters, 248, 750–758, doi:10.1016/j.epsl.2006.06.017, 2006.

Pimienta, P.: Etude du comportement mécanique des glaces polychristallines aux faibles contraintes ; applications aux glaces des calottes polaires, thèse, Université Joseph-Fourier - Grenoble I, 1987.

Pollard, D. and DeConto, R. M.: Modelling West Antarctic ice sheet growth and collapse through the past five million years, Nature, 458, 329–332, doi:10.1038/nature07809, 2009.

Pollard, D. and DeConto, R. M.: Description of a hybrid ice sheet-shelf model, and application to Antarctica, Geosci. Model Dev., 5, 1273–1295, doi:10.5194/gmd-5-1273-2012, 2012.

Pollard, D., DeConto, R. M., and Alley, R. B.: Potential Antarctic Ice Sheet retreat driven by hydrofracturing and ice cliff failure, Earth and Planetary Science Letters, 412, 112–121, doi:10.1016/j.epsl.2014.12.035, 2015.

Pritchard, H. D., Arthern, R. J., Vaughan, D. G., and Edwards, L. A.: Extensive dynamic thinning on the margins of the Greenland and Antarctic ice sheets, Nature, 461, 971–975, 2009.

Quiquet, A., Punge, H. J., Ritz, C., Fettweis, X., Gallée, H., Kageyama, M., Krinner, G., Salas y Mélia, D., and Sjolte, J.: Sensitivity of a Greenland ice sheet model to atmospheric forcing fields, The Cryosphere, 6, 999–1018, doi:10.5194/tc-6-999-2012, 2012.

Quiquet, A., Ritz, C., Punge, H. J., and Salas y Mélia, D.: Greenland ice sheet contribution to sea level rise during the last interglacial period: a modelling study driven and constrained by ice core data, Clim. Past, 9, 353–366, doi:10.5194/cp-9-353-2013, 2013.

Rignot, E., Jacobs, S., Mouginot, J., and Scheuchl, B.: Ice-Shelf Melting Around Antarctica, Science, 341, 266–270, doi:10.1126/science.1235798, 2013.

Ritz, C.: Un modèle thermo-mécanique d'évolution pour le bassin glaciaire antarctique Vostok-Glacier Byrd: Sensibilité aux valeurs des paramètres mal connus, thèse, Université Joseph-Fourier - Grenoble I, 1992.

Ritz, C., Fabre, A., and Letréguilly, A.: Sensitivity of a Greenland ice sheet model to ice flow and ablation parameters: consequences for the evolution through the last climatic cycle, Climate Dynamics, 13, 11–23, doi:10.1007/s003820050149, 1997.

Ritz, C., Rommelaere, V., and Dumas, C.: Modeling the evolution of Antarctic ice sheet over the last 420,000 years: Implications for altitude changes in the Vostok region, Journal of Geophysical Research, 106, 31 943–31 964, doi:10.1029/2001JD900232, 2001.

Ritz, C., Edwards, T. L., Durand, G., Payne, A. J., Peyaud, V., and Hindmarsh, R. C. A.: Potential sea-level rise from Antarctic ice-sheet instability constrained by observations, Nature, 528, 115–118, doi:10.1038/nature16147, 2015.

Roche, D. M., Dumas, C., Bügelmayer, M., Charbit, S., and Ritz, C.: Adding a dynamical cryosphere to iLOVECLIM (version 1.0): coupling with the GRISLI ice-sheet model, Geosci. Model Dev., 7, 1377–1394, doi:10.5194/gmd-7-1377-2014, 2014.

Rommelaere, V. and Ritz, C.: A thermomechanical model of ice-shelf flow, Annals of Glaciology, 23, 13–20, 1996.

Rybak, O. and Huybrechts, P.: A comparison of Eulerian and Lagrangian methods for dating in numerical ice-sheet models, Annals of Glaciology, 37, 150–158, doi:10.3189/172756403781815393, 2003.

Schoof, C.: Ice sheet grounding line dynamics: Steady states, stability, and hysteresis, Journal of Geophysical Research (Earth Surface), 112, 2007.

Shapiro, N. M. and Ritzwoller, M. H.: Inferring surface heat flux distributions guided by a global seismic model: particular application to Antarctica, Earth and Planetary Science Letters, 223, 213–224, doi:10.1016/j.epsl.2004.04.011, 2004.

Shreve, R. L.: Movement of Water in Glaciers, Journal of Glaciology, 11, 205–214, doi:10.3189/S002214300002219X, 1972.

Stone, E. J., Lunt, D. J., Rutt, I. C., and Hanna, E.: Investigating the sensitivity of numerical model simulations of the modern state of the Greenland ice-sheet and its future response to climate change, The Cryosphere, 4, 397–417, doi:10.5194/tc-4-397-2010, 2010.

Tsai, V. C., Stewart, A. L., and Thompson, A. F.: Marine ice-sheet profiles and stability under Coulomb basal conditions, Journal of Glaciology, 61, 205–215, doi:10.3189/2015JoG14J221, 2015.

Van Wessem, J., Reijmer, C., Morlighem, M., Mouginot, J., Rignot, E., Medley, B., Joughin, I., Wouters, B., Depoorter, M., Bamber, J., and et al.: Improved representation of East Antarctic surface mass balance in a regional atmospheric climate model, Journal of Glaciology, 60, 761–770, doi:10.3189/2014JoG14J051, 2014.

Waelbroeck, C., Labeyrie, L., Michel, E., Duplessy, J. C., McManus, J. F., Lambeck, K., Balbon, E., and Labracherie, M.: Sea-level and deep water temperature changes derived from benthic foraminifera isotopic records, Quaternary Science Reviews, 21, 295–305, doi:16/S0277-3791(01)00101-9, 2002.

Weertman, J.: On the Sliding of Glaciers, Journal of Glaciology, 3, 33–38, doi:10.3189/S0022143000024709, 1957.

Weertman, J.: Stability of the Junction of an Ice Sheet and an Ice Shelf, Journal of Glaciology, 13, 3–11, doi:10.3189/S0022143000023327, 1974.

Whitehouse, P. L., Bentley, M. J., and Le Brocq, A. M.: A deglacial model for Antarctica: geological constraints and glaciological modelling as a basis for a new model of Antarctic glacial isostatic adjustment, Quaternary Science Reviews, 32, 1–24, doi:10.1016/j.quascirev.2011.11.016, 2012.

Winkelmann, R., Martin, M. A., Haseloff, M., Albrecht, T., Bueler, E., Khroulev, C., and Levermann, A.: The Potsdam Parallel Ice Sheet Model (PISM-PIK) – Part 1: Model description, The Cryosphere, 5, 715–726, doi:10.5194/tc-5-715-2011, 2011.

Yan, Q., Zhang, Z., Gao, Y., Wang, H., and Johannessen, O. M.: Sensitivity of the modeled present-day Greenland Ice Sheet to climatic forcing and spin-up methods and its influence on future sea level projections, Journal of Geophysical Research: Earth Surface, 118, 2012JF002 709, doi:10.1002/jgrf.20156, 2013.

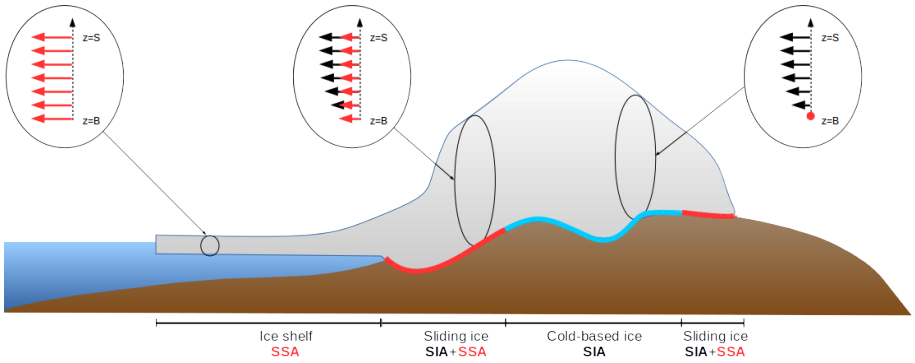

Figure 1. Schematic representation of the different types of flows in GRISLI and their associated velocity profiles. The red arrows stand for the sliding velocity which is non-zero for temperate-based grounded regions.

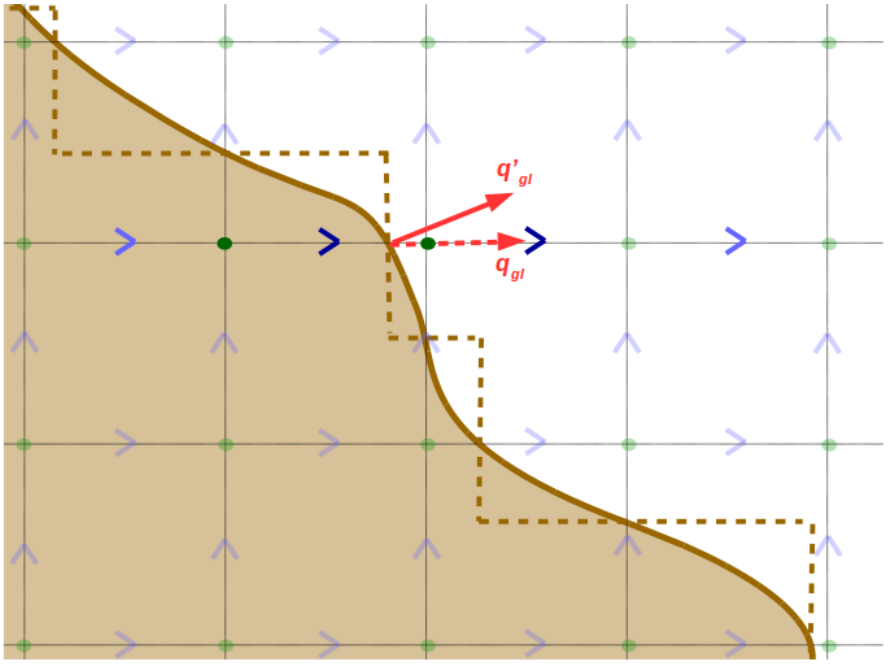

Figure 2. Horizontal staggered grids used in the model. The blue arrows stand for the staggered velocity grid while the green circles represent the standard centred grid (for, e.g., ice thickness, temperature, effective pressure). The plain brown line is an illustration of the grounding line position with an example of the flux (q'_{gl}) at one location where the grounding line crosses the x-axis in the centred grid. In the model, the norm of the flux at this location is reported on the u velocity only (q_{gl}), i.e. assuming a grounding line perpendicular to the x-axis (dashed brown line). The dark blue arrows are the velocity nodes on which q_{gl} is interpolated onto, using the velocity values of the two bounding light blue arrows. The dark green dots are used to infer the sub-grid position of the grounding, interpolating the floatation criterion ($\rho H + \rho_w (B - sealevel)$).

Table 1. GRISLI model parameters used in this study.

Variable	Identifier name	Value
Global constants		
Gravitational acceleration	g	$9.81\,\mathrm{m\,s^{-2}}$
Water density, liquid	ρ_w	$1000\,\mathrm{kg\,m^{-3}}$
Water density, ice	ρ	$918\,\mathrm{kg\,m^{-3}}$
Water density, ocean	ρ_o	$1028\,\mathrm{kg\,m^{-3}}$
Isostasy		
Mantle density	ρ_m	$3300\,\mathrm{kg\,m^{-3}}$
Relaxation time in isostasy	τ_m	$3000\,\mathrm{yr}$
Lithosphere flexural rigidity	D_l	$9.87 \times 10^{24}\,\mathrm{N\,m}$
Radius of relative stiffness	R_l	$131910\,\mathrm{m}$
Radius of action of a unit mass	R_{iso}	$400\,\mathrm{km}$
Hydrology		
Thickness of the till layer	h_{till}	$20\,\mathrm{m}$
Porosity of the till layer	ϕ_{till}	0.5
Deformation		
Transition temperature of deformation, Glen	T_3^{trans}	$-6.5\,^\circ\mathrm{C}$
Activation energy below transition, Glen	$E_{a\ 3}^{\mathrm{cold}}$	$7.820 \times 10^4\,\mathrm{J\,mol^{-1}}$
Activation energy above transition, Glen	$E_{a\ 3}^{\mathrm{warm}}$	$9.545 \times 10^4\,\mathrm{J\,mol^{-1}}$
Flow law coefficient below transition, Glen	$B_{AT0\ 3}^{\mathrm{cold}}$	$1.660 \times 10^{-16}\,\mathrm{Pa^{-3}\,yr^{-1}}$
Flow law coefficient above transition, Glen	$B_{AT0\ 3}^{\mathrm{warm}}$	$2.000 \times 10^{-16}\,\mathrm{Pa^{-3}\,yr^{-1}}$
Transition temperature of deformation, linear	T_1^{trans}	$-10\,^\circ\mathrm{C}$
Activation energy below transition, linear	$E_{a\ 1}^{\mathrm{cold}}$	$4.0 \times 10^4\,\mathrm{J\,mol^{-1}}$
Activation energy above transition, linear	$E_{a\ 1}^{\mathrm{warm}}$	$6.0 \times 10^4\,\mathrm{J\,mol^{-1}}$
Flow law coefficient below transition, linear	$B_{AT0\ 1}^{\mathrm{cold}}$	$8.373 \times 10^{-8}\,\mathrm{Pa^{-3}\,yr^{-1}}$
Flow law coefficient above transition, linear	$B_{AT0\ 1}^{\mathrm{warm}}$	$8.373 \times 10^{-8}\,\mathrm{Pa^{-3}\,yr^{-1}}$
Temperature		
Gas constant	R	$8.314\,\mathrm{J\,mol^{-1}\,K^{-1}}$
Ice melting temperature, at depth z	T_m	$9.35 \times 10^{-5} \rho g (S - z)\,\mathrm{K\,kPa^{-1}}$
Latent heat of ice fusion	L_f	$335 \times 10^3\,\mathrm{J\,kg^{-1}}$
Ice thermal conductivity, at temperature T	k_i	$3.1014 \times 10^8 \exp(-0.0057\,(T + 273.15))\,\mathrm{J\,m^{-1}K^{-1}yr^{-1}}$
Mantle thermal conductivity	k_b	$1.04 \times 10^8\,\mathrm{J\,m^{-1}K^{-1}yr^{-1}}$

Table 2. Selected parameters included in the latin hypercube sampling (LHS) ensemble with their associated ranges.

Parameter	Units	Minimum	Maximum
~~E_{STA}~~ S_f	–	1.	5.
C_f	~~$yr\ m^{-1}$~~ $\mathrm{yr\,m^{-1}}$	$0.5\ 10^{-3}$	$5.\ 10^{-3}$
K_0	~~$m\ yr^{-1}$~~ $\mathrm{m\,yr^{-1}}$	20.10^{-6}	200.10^{-6}
b_{melt}	–	0.75	1.25

Table 3. Parameter values for the ensemble members that yield the lowest RMSE with respect to observations at the end of 100-kyr simulation under perpetual present-day climate forcing.

	ensemble member	S_f	C_f ($\mathrm{yr\,m^{-1}}$)	K_0 ($\mathrm{m\,yr^{-1}}$)	ϕ_{shelf}
Using Schoof (2007)	123	3.19	$2.4\ 10^{-3}$	$188\ 10^{-6}$	1.05
Using Tsai et al. (2015)	213	2.33	$4.6\ 10^{-3}$	$114\ 10^{-6}$	0.86

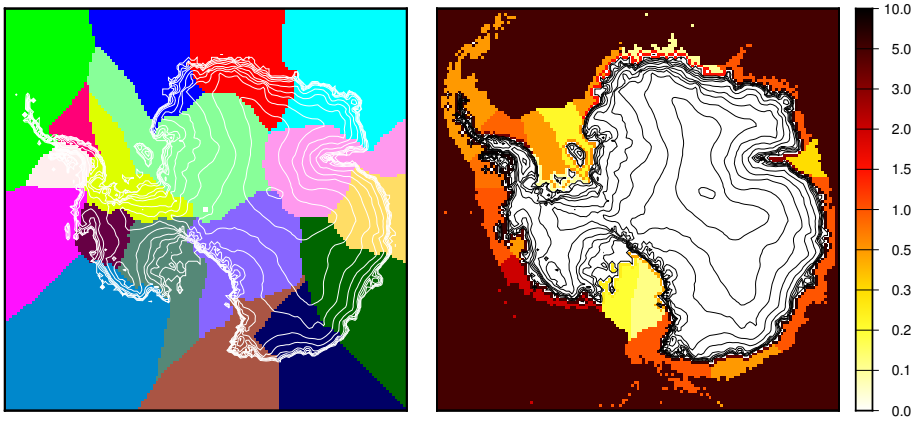

Figure 3. Antarctic ice shelves sectors (left) and associated prescribed present-day sub-shelf basal melting rates in $\mathrm{m\,yr^{-1}}$ (right). The melting rates are different for the shelf and the associated grounding line to mimic the higher values observed close to the grounding line (Rignot et al., 2013). Sub-shelf melting rate for the deep ocean (depth greater than 2500 m) are assigned a value of $5\,\mathrm{m\,yr^{-1}}$.

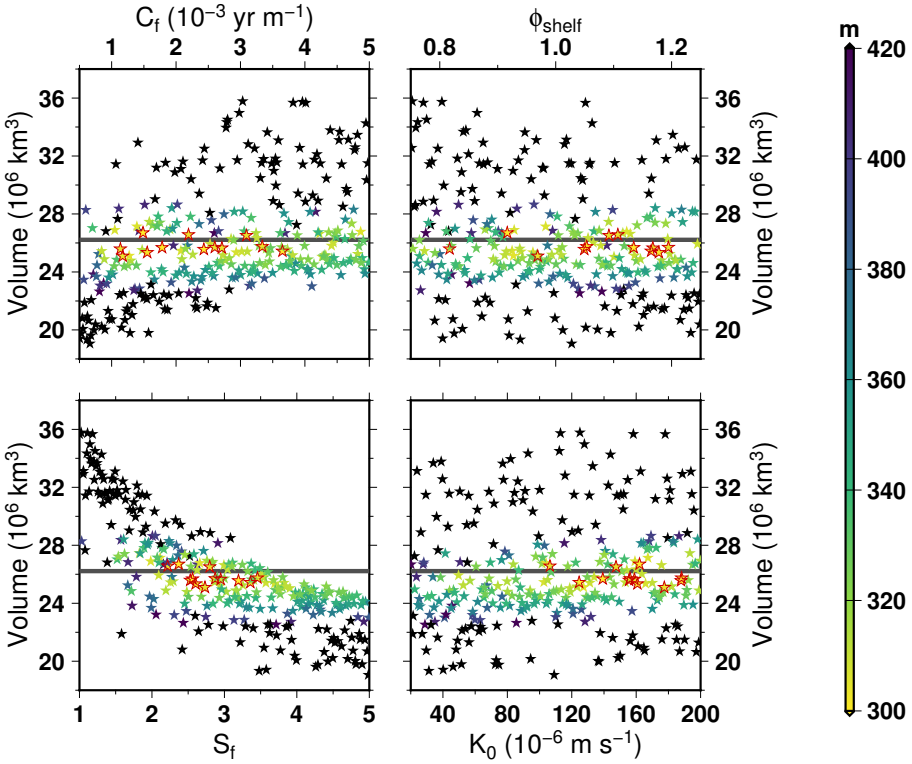

Figure 4. Simulated total ice volume for each ensemble members as a function of parameter values when using the Schoof (2007) formulation of the flux at the grounding line (AN40S). The thick horizontal line stands for the observations (Fretwell et al., 2013). The colour shading corresponds to the root mean square error in ice thickness relative to observations. The stars outlined in red are the 12 ensemble members that yield the lowest RMSE.

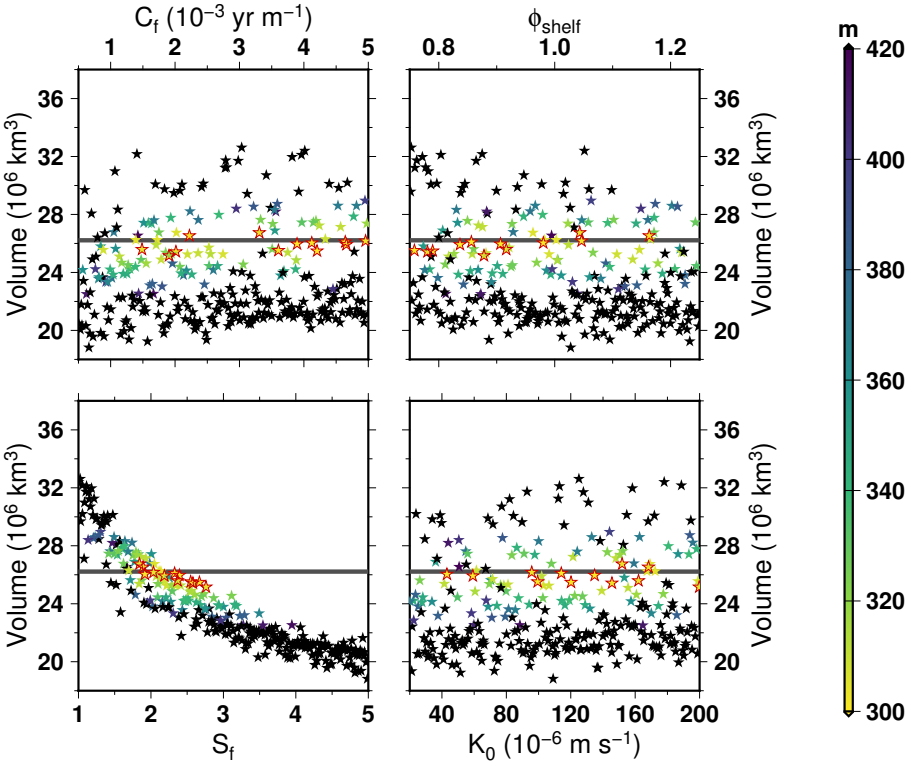

Figure 5. Same as Fig. 4 but with the Tsai et al. (2015) formulation of the flux at the grounding line (AN40T).

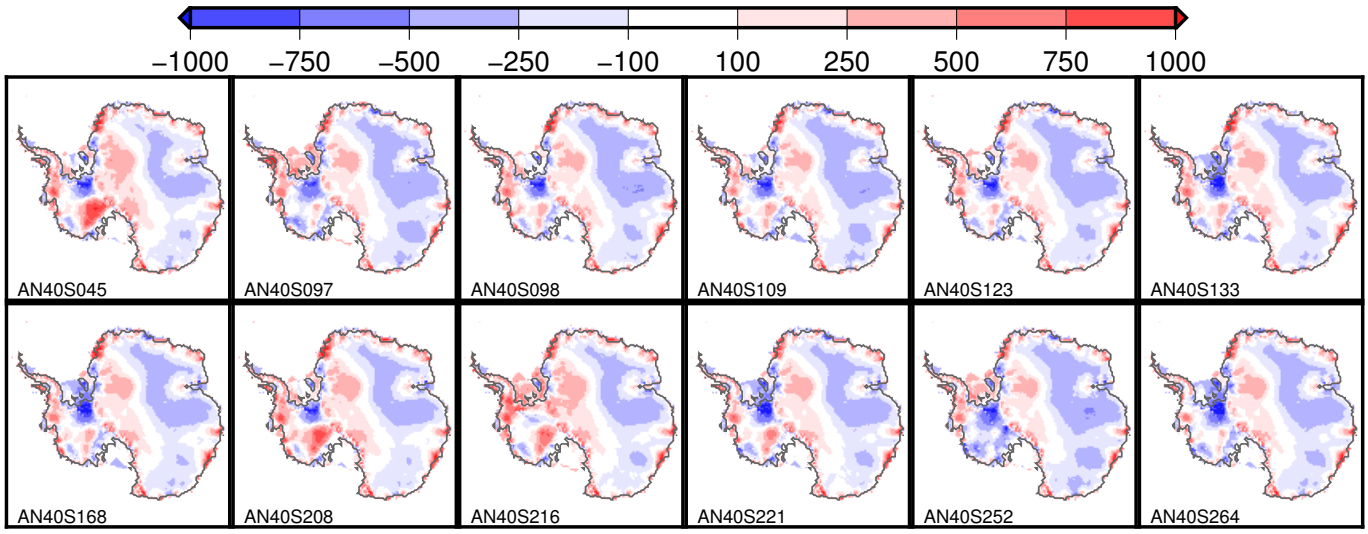

Figure 6. Ice thickness difference with the observations (simulated minus observed) from the 12 ensemble members showing the lowest RMSE when using the Schoof (2007) formulation of the flux at the grounding line (AN40S).

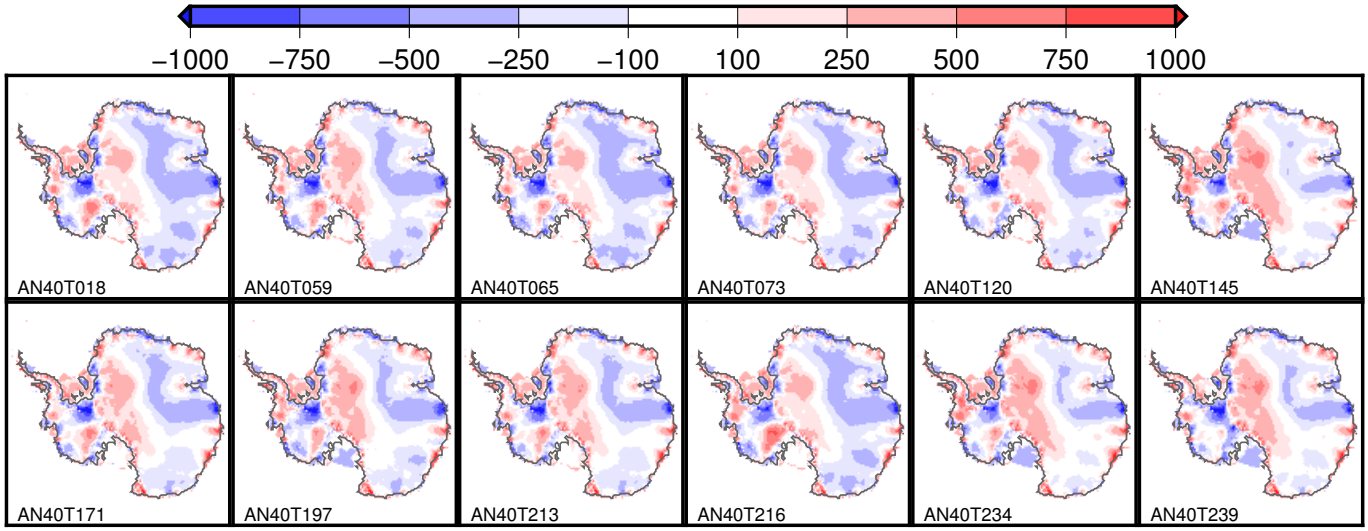

Figure 7. Same as Fig. 6 but with the Tsai et al. (2015) formulation of the flux at the grounding line (AN40T).

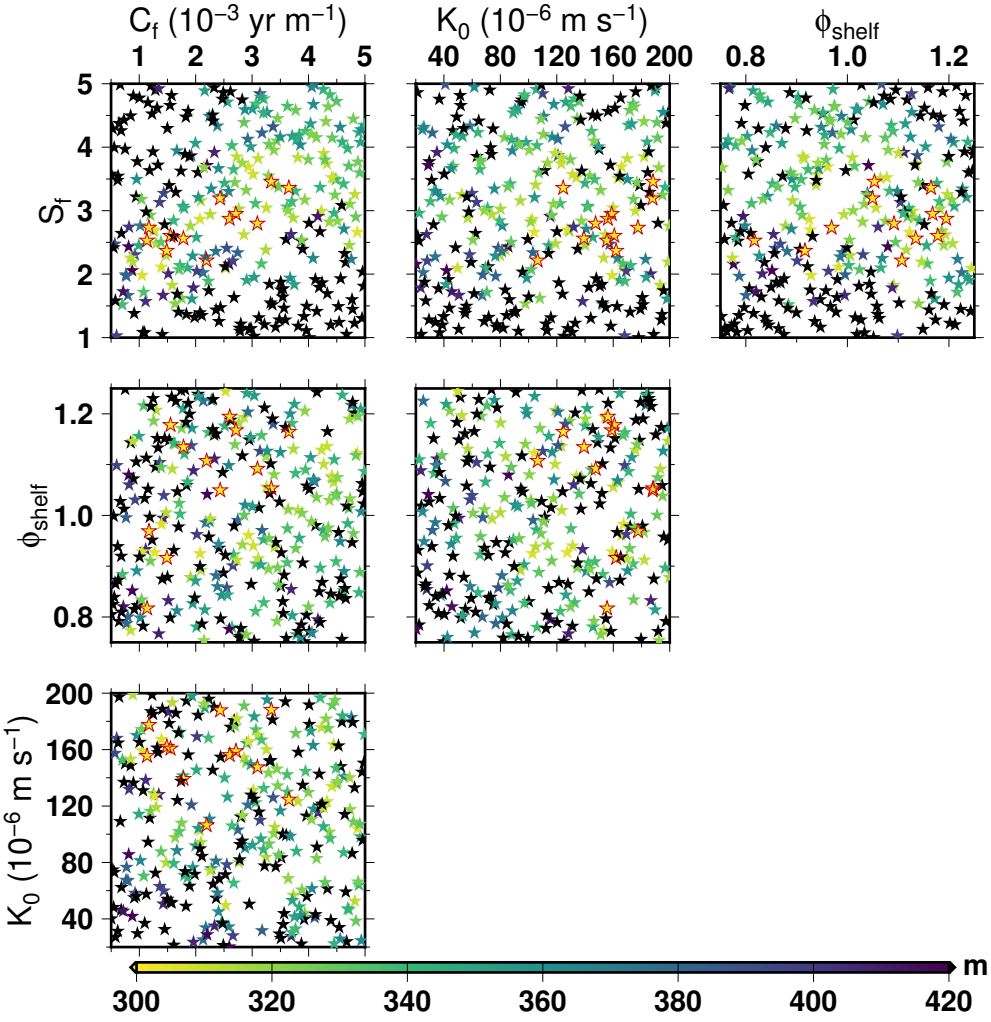

Figure 8. Ice thickness root mean square error respective to observations in the parameter space for the 300 model members using the Schoof (2007) formulation of the flux at the grounding line (AN40S). The 12 experiments showing the lowest error are outlined in red.

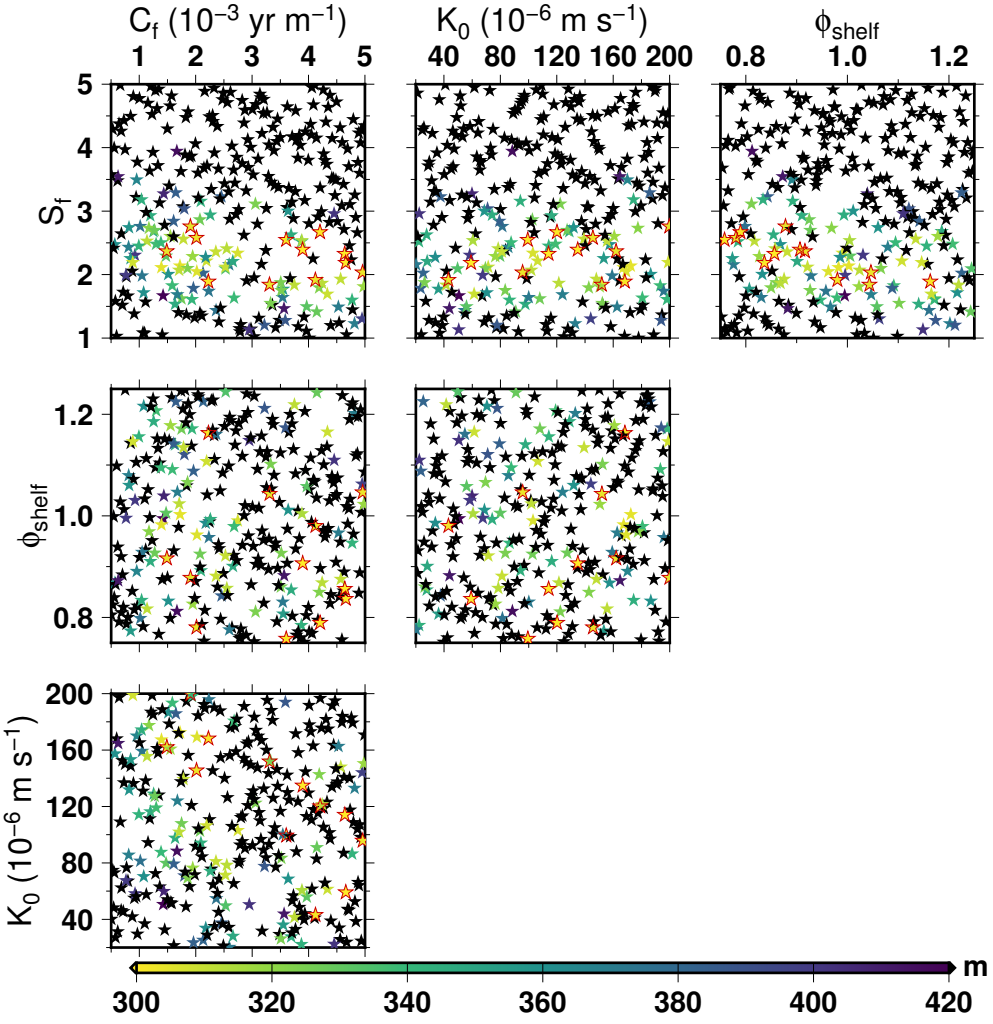

Figure 9. Same as Fig. 8 but with the Tsai et al. (2015) formulation of the flux at the grounding line (AN40T).

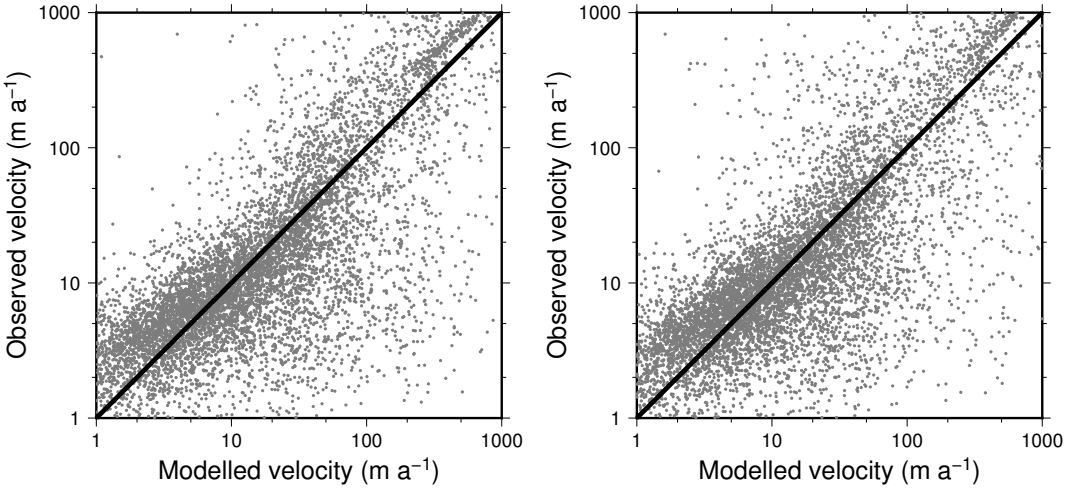

Figure 10. Observed velocity (Mouginot et al., 2017) against modelled velocity on the 40 km grid. Only the best ensemble members with the lowest RMSE is shown here for Schoof (2007) (AN40S123, left) and Tsai et al. (2015) (AN40T213, right). The parameter values for these experiments are shown in Tab. 3.

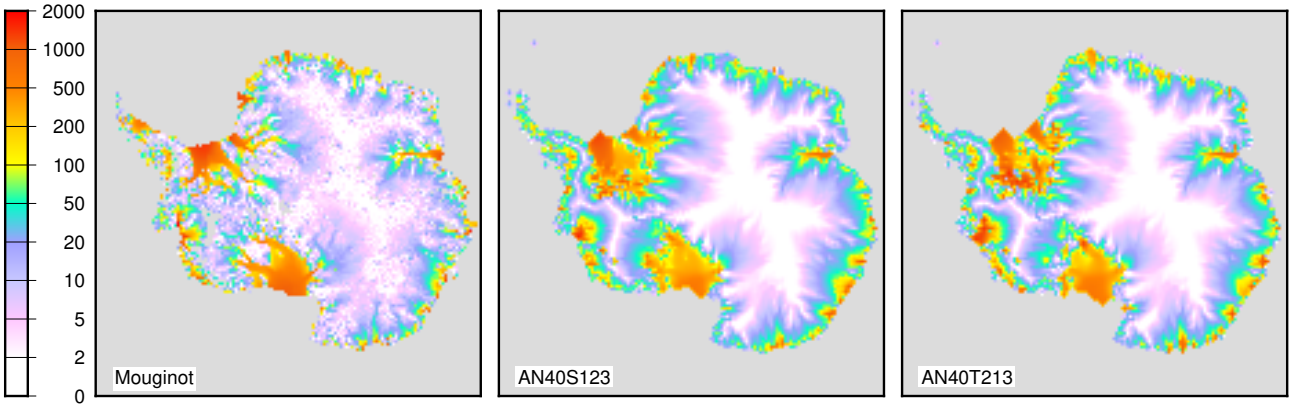

Figure 11. Map of observed (Mouginot et al., 2017) and simulated velocities in $\mathrm{m\,yr^{-1}}$ for the ensemble members with the lowest RMSE using Schoof (2007) (AN40S123) and Tsai et al. (2015) (AN40T213).

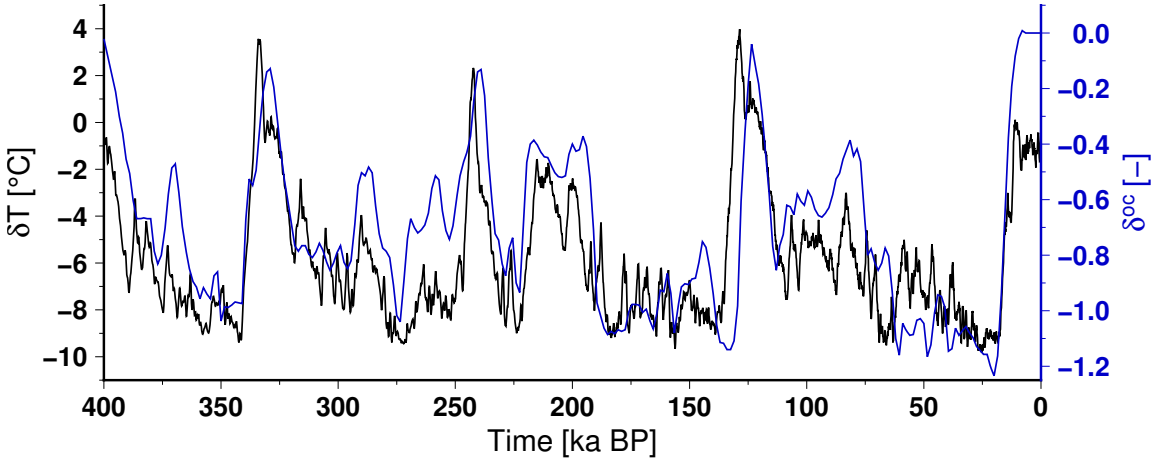

Figure 12. Climatic perturbation used in the 400 kyr glacial-interglacial simulations for the near-surface air temperature, $\delta T = \left(1/\alpha^{i}\right)\delta D$, and for the sub-shelf basal melting rate modificator, $\delta^{oc} = \alpha^{oc}\,\Delta T_{NA}/T_{NA0}$.

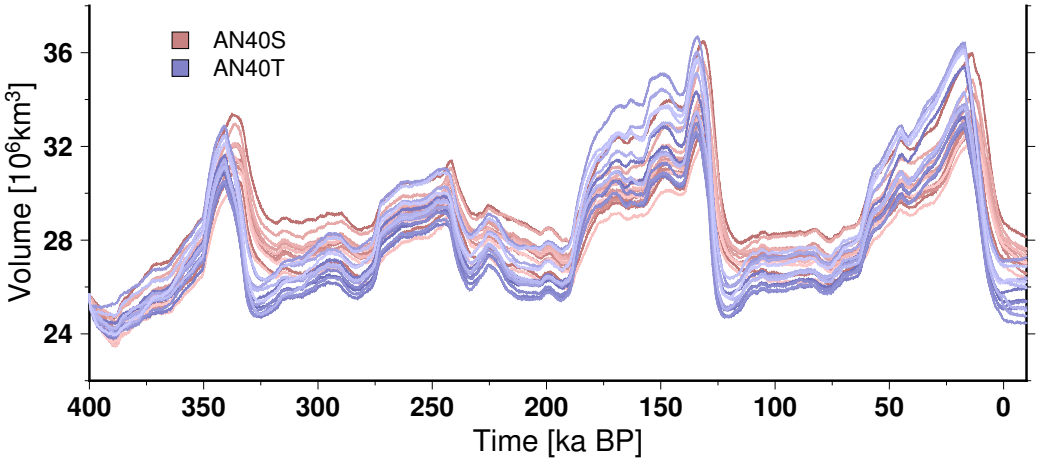

Figure 13. Simulated total ice sheet volume evolution over the last 400 kyr for the twelve ensemble members showing the lowest RMSE in Sec. 3 when using the flux at the grounding line computed from Schoof (2007) (AN40S, shade of reds) and Tsai et al. (2015) (AN40T, shade of blues). The glacial to interglacial difference in ice volume for the last termination corresponds to about -10 to -20 m of global sea level rise equivalent depending on the simulations.

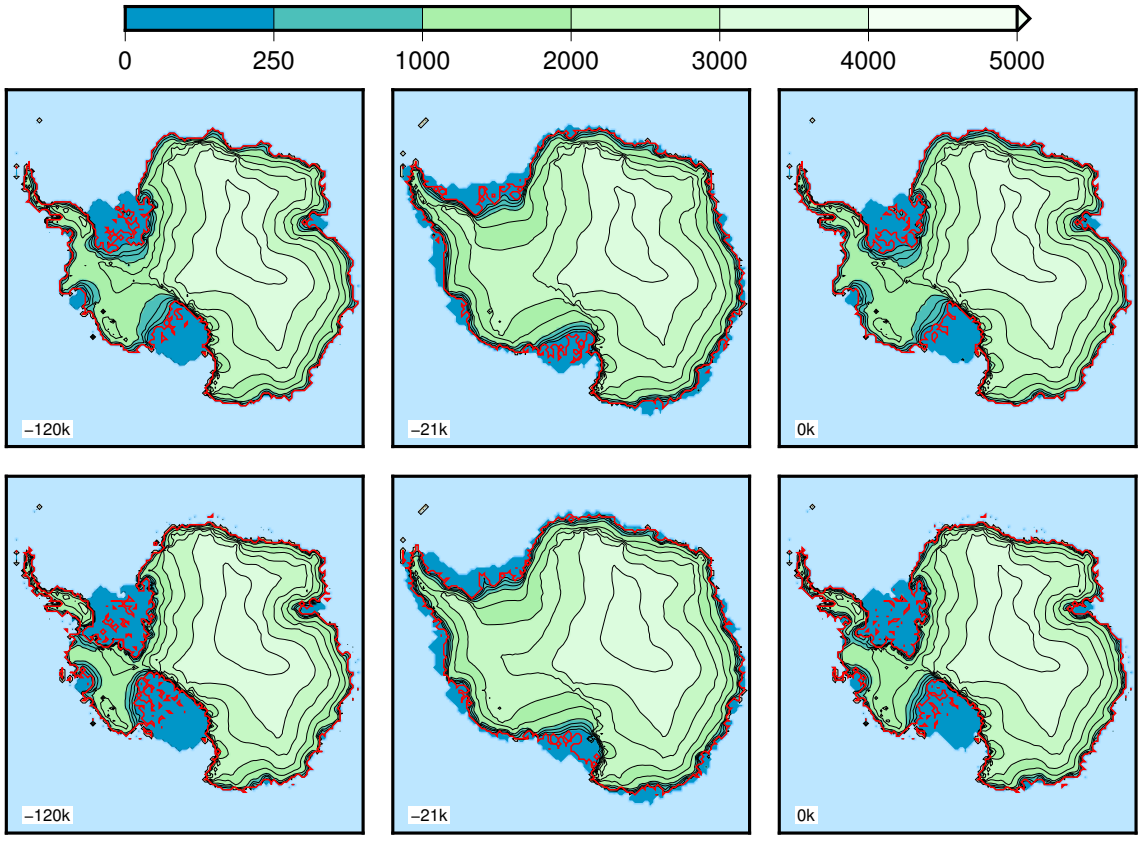

Figure 14. Simulated surface elevation at selected snapshots for the two ensemble members that produce the minimal RMSE at 0 kaBP in the transient simulations (AN40S252, top, and AN40T213, bottom). The ice volume contributing to sea level change from present is -9.3 m (resp. -15.1 m) at 21 kaBP for AN40S252 (resp. AN40T213), whilst it is limited at 120 kaBP (-0.3 m and +0.6 m). The grounding line is indicated by the thick red line.

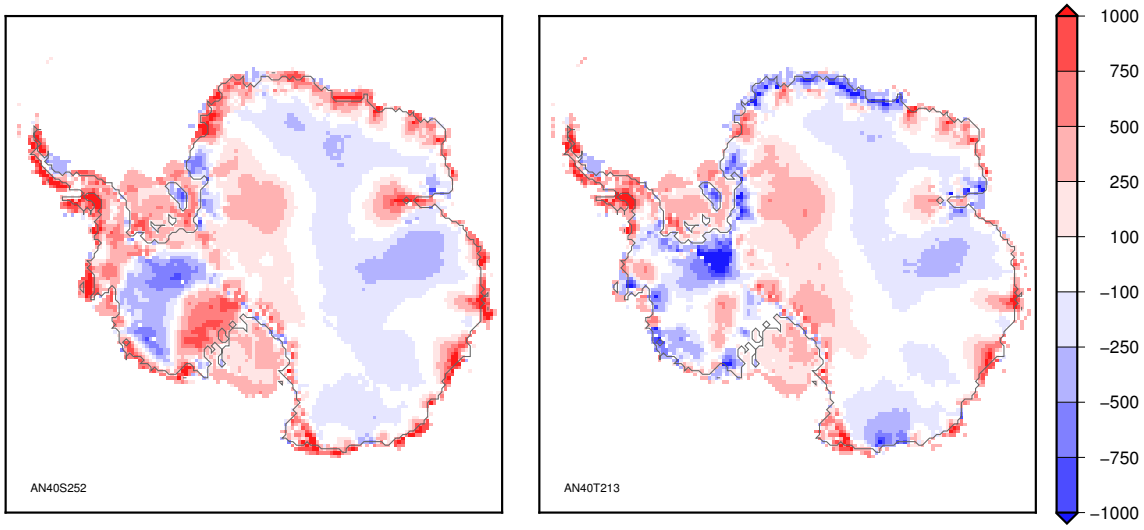

Figure 15. Ice thickness difference with the observations (simulated minus observed) at 0 ka BP for the two ensemble members that produce the minimal RMSE at 0 kaBP in the transient simulations (AN40S252, left, and AN40T213, right). The RMSE is 350 m (respectively 313 m) for AN40S252 (resp. AN40T213).